An anisotropic elastoplastic model for soft clays based on logarithmic contractancy

by

Nallathamby Sivasithamparam ([1]) and Jorge Castro ([2])(*)

E-mail: ([1]) nallathamby.siva@ngi.no ([2]) castrogj@unican.es

([1]) Computational Geomechanics Division, Norwegian Geotechnical Institute, Oslo, Norway

([2]) Lecturer, Department of Ground Engineering and Materials Science, University of Cantabria, Santander, Spain

(*) Corresponding author:

Group of Geotechnical Engineering
Department of Ground Engineering and Materials Science
University of Cantabria
Avda. de Los Castros, s/n
39005 Santander, Spain
Tel.: +34 942 201813
Fax: +34 942 201821
e-mail: castrogj@unican.es

Date: June 2015

Number of words: 6,300

Number of tables: 1

Number of figures: 20

Abstract

A new constitutive model for soft structured clays is developed based on an existing model called S-CLAY1S, which is a Cam Clay type model that accounts for anisotropy and destructuration. The new model (E-SCLAY1S) uses the framework of logarithmic contractancy to introduce a new parameter that controls the shape of the yield surface as well as the plastic potential (as an assumed associated flow rule is applied). This new parameter can be used to fit the coefficient of earth pressure at rest, the undrained shear strength or the stiffness under shearing stress paths predicted by the model. The improvement to previous constitutive models that account for soil fabric and bonding is formulated within the contractancy framework such that the model predicts the uniqueness of the critical state line and its slope is independent of the contractancy parameter. Good agreement has been found between the model predictions and published laboratory results for triaxial compression tests. An important finding is that the contractancy parameter, and consequently the shape of the yield surface, seem to change with the degree of anisotropy; however, further study is required to investigate this response. From published data, the yield surface for isotropically consolidated clays seems “bullet” or “almond” shaped, similar to that of the Cam Clay model; while for anisotropically consolidated clays, the yield surface is more elliptical, like a rotated and distorted Modified Cam Clay yield surface.

Keywords: constitutive modelling; soft soils; critical state; anisotropy; logarithmic contractancy; yield surface.

1. Introduction

Extensive experimental testing of soils under different stress paths and conditions as well as the increase in computing power have led to the development of advanced constitutive models that reproduce more accurately the mechanical behaviour of soils. Since the pioneering work of Roscoe and co-workers [1-3], many constitutive models have been proposed in the framework of Critical State soil mechanics. The first Critical State model was the (original) Cam Clay model, whose plastic potential surface was obtained on the basis of assuming a simple frictional form for the plastic work. Associated flow conditions were assumed and therefore, the yield and plastic potential surfaces coincide.

The original model was modified (Modified Cam Clay) [4] using a different formulation of the dissipated energy during plastic straining to get an elliptical yield surface that overcomes some of the limitations of the original surface, e.g. the singularity on the mean effective stress axis (q=0). Further yield and plastic potential surfaces have been proposed in the literature since then, e.g. [5,6]. Hence, the shapes of the yield and plastic potential surfaces vary from model to model. A constitutive model that is able to reproduce a variety of shapes (yield surfaces) could provide predictions that are more accurate. Following that idea, Lagioia et al. [7] developed a versatile expression for the yield and plastic potential surfaces based on a mathematical relation between the dilatancy and the stress ratio. However, this model is limited to isotropic soils and does not account for natural soil features such as fabric and some apparent bonding that will be progressively lost during loading.

Natural soft soil deposits exhibit inherent anisotropic behaviour due to its deposition history. Therefore, the extent of anisotropy can be modelled by a rotated and distorted elliptical yield surface (e.g. Dafalias [8], S-CLAY1 model [9], MIT-E3 model [10] or Sekiguchi-Ohta model [11]) by considering inter-dependence (coupling) of volumetric and deviatoric plastic strains in the plastic work equation. The major differences between these models are shape of the yield surface and rotational hardening rule. The S-CLAY1 model [9] was further extended to include soil structure (S-CLAY1S [12]) through an intrinsic yield surface. The S-CLAY1S model has proven its ability to reproduce the behaviour of normally or slightly overconsolidated structured soft clays [12-15]. Despite its good performance, especially for settlement prediction, horizontal displacements are generally not well matched, e.g. [15]. Those differences may be attributed to the shape of the yield surface (i.e. associates with flow rule), or similarly, to the horizontal/vertical stress ratio predicted by the model for compression loading.

Ohta et al. [16] presented a unified framework for different shapes of the yield surface, assuming associated flow conditions. The framework is based on curve fitting of experimental results of the contractancy (compressive volumetric strain, ε_v) during drained shear at constant mean effective stress (p') of normally consolidated clays. Those experimental results were first presented by Shibata [17]. Ohno et al. [18] proposed two categories of contractancy models, namely exponential and logarithmic contractancy models, depending on the type of function used to fit the experimental results. (Original) Cam Clay (CC) and Modified Cam Clay (MCC) models are particular cases of the general contractancy models. Ohta et al. [16] extended the contractancy models to anisotropic conditions using the stress parameter introduced by Sekiguchi and Ohta [11]. Therefore, they are called Extended Sekiguchi-Ohta models [16]. These

models do not account for evolution of anisotropy with loading and apparent bonding of natural soils. Further, the Extended Sekiguchi-Ohta models fail to predict unique critical state line (CSL) as for example in triaxial compression and extension in p'- q space.

According to Dafalias and Taiebat [19], introducing a non-associated flow rule can provide improved predictions regardless of the rotational hardening rule employed while it is able to obtain unique CSL. However, the introduction of a non-associated flow rule may be either not necessary or convenient. Therefore, development of an adequate but simple constitutive model for anisotropic and structured clays is still relevant.

This paper extends the S-CLAY1S model [12] using the framework of logarithmic contractancy [16] to include some flexibility in the shape of the yield surface. The new model introduces an additional parameter, called the contractancy parameter, which controls the shape of the yield surface. The contractancy parameter can be related to the coefficient of earth pressure at rest for normally consolidated conditions, K_{0NC}, the undrained shear strength, c_u, or the stiffness under shearing stress paths. In this way, the proposed model, called E-SCLAY1S, extends the predictive capabilities of the S-CLAY1S model, while including just an additional parameter with clear physical meaning.

The paper presents the formulation of the new model (Section 2) and its numerical implementation (Section 3). Section 4 highlights the main features of the model, such as the slope and uniqueness of the CSL and the influence of the contractancy parameter on the coefficient of earth pressure, the undrained shear strength, the yield surface and the

soil stiffness. The model is validated against laboratory tests on two clays, namely Kaolin clay and Santa Clara clay (Section 5) and finally some discussion and conclusions are provided.

2. Proposed model: E-SCLAY1S

The proposed model extends S-CLAY1S [12], which is a Modified Cam Clay [4] type model that accounts for anisotropy and destructuration. Anisotropy of plastic behaviour is represented through an inclined and distorted yield surface and a rotational hardening law to model the development or erasure of fabric anisotropy during plastic straining; while interparticle bonding and degradation of bonds (structure) is reproduced using intrinsic and natural yield surfaces [20] and a hardening law describing destructuration as a function of plastic straining. For the sake of simplicity, the mathematical formulation is presented in the following in triaxial stress space, which can be used only to model the response of cross-anisotropic samples (cut vertically from the soil deposit) subject to oedometer or triaxial loading. The original inclined yield surface of the S-CLAY1S model is elliptical [8] (see Figure 1):

$$f_y = 1 + \frac{(\eta - \alpha)^2}{M^2 - \alpha^2} - \frac{p'_m}{p'} = 0 \tag{1}$$

The above yield function often cannot describe experimental data of yield points with enough accuracy as well as undrained stress paths [19]. An improvement can be achieved by modifying the yield function. The proposed model (E-SCLAY1S) introduces a degree of freedom in the shape of the yield surface (Eq. 1) using the framework of logarithmic contractancy [16] (see Appendix I):

$$f_y = \left(1 + \frac{\left|\eta - \alpha\right|^{n_L}}{M^{n_L} - \alpha^{n_L}} \right)^{\Psi} - \frac{p'_m}{p'} = 0 \tag{2}$$

where Ψ is an intermediate parameter to simplify Eq. (2)

$$\Psi = \frac{(M - \alpha)}{n_L M} \left[1 + \frac{M^{n_L} - \alpha^{n_L}}{(M - \alpha)^{n_L}} \right] \tag{3}$$

and n_L is a new parameter (contractancy parameter) that controls the shape of the yield surface. The subscript "*L*" refers to logarithmic contractancy, following the notation by Ohta et al. [16]. So, the shape of the yield surface in the E-SCLAY1S model depends on the contractancy parameter, n_L (see Figures 2 and 3). It is worth mentioning that it corresponds to the shape of both the natural and intrinsic yield surfaces and also the plastic potential surface, since an associated flow rule is assumed. For the sake of brevity, hereafter it is referred to as the yield surface. The E-SCLAY1S preserves the hierarchical development of S-CLAY1S, as the former reduces to the later for n_L=2, i.e. Eq. (2) reduces to Eq. (1) as Ψ=1.

The shape of yield surfaces may be classified as:

- "Bullet" or "almond" shape (e.g. original Cam Clay)
- Elliptical (e.g. Modified Cam Clay)
- "Tear" or "Sheared" shape (e.g. Lade and Kim [6])

For the E-SCLAY1S model, and in general for logarithmic contractancy models, the yield surface is elliptical for n_L=2, "bullet" shaped for n_L<2 and "tear" shaped for n_L>2. Most of the anisotropic models (e.g. S-CLAY1S and MIT-E3) use elliptical surfaces, but empirical evidences show the limitations associated with elliptical yield surfaces

(e.g. [21]). Similarly to (original) Cam Clay model, the yield surfaces for n_L<2 have a singularity at $\eta=\alpha$ (Figure 2).

As in the S-CLAY1S model, the effect of bonding in the E-SCLAY1S model is described by an intrinsic yield surface [20], which has the same shape and inclination of the natural yield surface but with a smaller size (see Figure 1). The size of the intrinsic yield surface is specified by the state parameter p'_{mi}, which is related to the size p'_m of the natural yield surface by the state parameter χ as the current amount of bonding

$$p'_m = (1+\chi)\, p'_{mi} \tag{4}$$

The last letter of the model ("S") refers to the soil structure. So, when the hierarchical version of the model without destructuration is used, the model is simply called E-SCLAY1.

The three hardening rules of the original S-CLAY1S model, namely isotropic hardening, rotational hardening and degradation of bonds rule, are kept as the original [9, 12]. The first rule relates the increase in the size of the intrinsic yield surface to the increments of plastic volumetric strain ($d\varepsilon_v^p$)

$$dp'_{mi} = \frac{v p'_{mi}}{\lambda_i - \kappa} d\varepsilon_v^p \tag{5}$$

where v is the specific volume, λ_i is the gradient of the intrinsic normal compression line in the compression plane ($\ln p' - v$ space), and κ is the slope of the swelling line in the compression plane.

The second hardening law is the rotational hardening law, which describes the rotation of the yield surface with plastic straining

$$d\boldsymbol{\alpha}_{\mathbf{d}} = \omega\left[\left(\frac{3\boldsymbol{\eta}}{4} - \boldsymbol{\alpha}_{\mathbf{d}}\right)\left\langle d\varepsilon_v^p \right\rangle + \omega_d\left(\frac{\boldsymbol{\eta}}{3} - \boldsymbol{\alpha}_{\mathbf{d}}\right)\left|d\varepsilon_d^p\right|\right] \tag{6}$$

where $\boldsymbol{\eta}$ is the tensorial equivalent of the stress ratio defined as $\boldsymbol{\eta} = \boldsymbol{\sigma}_{\mathbf{d}} / p'$, $d\varepsilon_d^p$ is the increment of plastic deviatoric strain, $\boldsymbol{\alpha}_{\mathbf{d}}$ is the deviatoric fabric tensor, which has the same form as the deviatoric stress vector [9], and ω and ω_d are additional soil constants that control rotational hardening.

The third law for destructuration is formulated in such a way that both plastic volumetric strains and plastic shear strains tend to decrease the value of the bonding parameter χ towards a target value of zero, it is defined as

$$d\chi = -\xi\chi\left(\left|d\varepsilon_v^p\right| + \xi_d\left|d\varepsilon_d^p\right|\right) \tag{7}$$

where ξ and ξ_d are additional soil constants. As full details of the hardening laws and determination of the soil constants is beyond the scope of this paper, they can be found in [9, 12].

The extension of the model from triaxial stress space to general (multiaxial) stress space is also equivalent to that of S-CLAY1S [22]. The model has been implemented using the Euler backward implicit integration scheme [22], in such a way that it can be incorporated directly into finite element codes (e.g. PLAXIS [23]) for engineering applications. The implementation is presented in the following section.

3. Discretization and numerical implementation

The decomposition of total strains in classical elasto-plastic theory using an additive rule can be expressed in terms of elastic and plastic components of strains as

$$d\boldsymbol{\varepsilon} = d\boldsymbol{\varepsilon}^{e} + d\boldsymbol{\varepsilon}^{p} \tag{8}$$

where d remarks an incremental operator, the boldface characters are used to denote tensor quantities and superscript "*e*" denotes the elastic component and "*p*" denotes the plastic component.

The plastic strain increment can be calculated using the plastic multiplier ($d\Lambda$)

$$d\boldsymbol{\varepsilon}^{p} = d\Lambda \frac{\partial f_y}{\partial \boldsymbol{\sigma}'} \tag{9}$$

The plastic potential is the yield function because an associated flow rule is assumed.

To derive the plastic multiplier of the E-SCLAY1S model, the consistency condition of the yield function ($df_y = 0$) is used

$$df_y = \frac{\partial f_y}{\partial \boldsymbol{\sigma}'} d\boldsymbol{\sigma}' + \frac{\partial f_y}{\partial p'_{mi}} dp'_{mi} + \frac{\partial f_y}{\partial \boldsymbol{\alpha}} d\boldsymbol{\alpha} + \frac{\partial f_y}{\partial \chi} d\chi = 0 \tag{10}$$

By substituting stress increment and isotropic, rotational hardening rules as well as destructuration law, the plastic multiplier is derived as

$$d\Lambda = \frac{\left\{\frac{\partial f_y}{\partial \boldsymbol{\sigma}'}\right\}^{T} \boldsymbol{D}_e d\boldsymbol{\varepsilon}}{\left\{\frac{\partial f_y}{\partial \boldsymbol{\sigma}'}\right\}^{T} \boldsymbol{D}_e \left\{\frac{\partial f_y}{\partial \boldsymbol{\sigma}'}\right\} + H_0 + H_\alpha + H_\chi} \tag{11}$$

where elastic stiffness matrix $\boldsymbol{D}_e$ is

$$\boldsymbol{D}_e = \begin{bmatrix} 2G\frac{1-\nu'}{1-2\nu'} & 2G\frac{\nu'}{1-2\nu'} & 2G\frac{\nu'}{1-2\nu'} & 0 & 0 & 0 \\ 2G\frac{\nu'}{1-2\nu'} & 2G\frac{1-\nu'}{1-2\nu'} & 2G\frac{\nu'}{1-2\nu'} & 0 & 0 & 0 \\ 2G\frac{\nu'}{1-2\nu'} & 2G\frac{\nu'}{1-2\nu'} & 2G\frac{1-\nu'}{1-2\nu'} & 0 & 0 & 0 \\ 0 & 0 & 0 & G & 0 & 0 \\ 0 & 0 & 0 & 0 & G & 0 \\ 0 & 0 & 0 & 0 & 0 & G \end{bmatrix} \tag{12}$$

where $G = \frac{3}{2}\left(\frac{1-2\nu'}{1+\nu'}\right)\left(\frac{1+e_0}{\kappa}\right)p'$ and ν' is Poisson's ratio.

For a small increment in implicit integration scheme, it can be further simplified in terms of value of yield function (f_y^0) as

$$d\Lambda = \frac{f_y^0}{\left\{\frac{\partial f_y}{\partial \boldsymbol{\sigma}'}\right\}^T \boldsymbol{D}_e \left\{\frac{\partial f_y}{\partial \boldsymbol{\sigma}'}\right\} + H_0 + H_\alpha + H_\chi} \tag{13}$$

where superscript T corresponds to a matrix transpose and hardening moduli H_0, H_α and H_χ are derived as

$$H_0 = -p'(1+\chi)p'_{mi}\left(\frac{1+e_0}{\lambda_i - \kappa}\right)\frac{\partial f_y}{\partial p'} \tag{14}$$

$$H_\alpha = \left\{\frac{\partial f_y}{\partial \boldsymbol{\alpha}_d}\right\}^T \left[\frac{\partial \boldsymbol{\alpha}_d}{\partial \varepsilon_v^p}\left\langle\frac{\partial f_y}{\partial p'}\right\rangle + \frac{\partial \boldsymbol{\alpha}_d}{\partial \varepsilon_d^p}\sqrt{\frac{3}{2}\left\{\frac{\partial f_y}{\partial \boldsymbol{\sigma}'_d}\right\}^T \left\{\frac{\partial f_y}{\partial \boldsymbol{\sigma}'_d}\right\}}\right] \tag{15}$$

$$\mathrm{H}_\chi = \frac{\partial f_y}{\partial \chi}\left[\frac{\partial \chi}{\partial \varepsilon_v^p}\left\langle\frac{\partial f_y}{\partial p'}\right\rangle + \frac{\partial \chi}{\partial \varepsilon_d^p}\sqrt{\frac{3}{2}\left\{\frac{\partial f_y}{\partial \boldsymbol{\sigma}'_d}\right\}^T \left\{\frac{\partial f_y}{\partial \boldsymbol{\sigma}'_d}\right\}}\right] \tag{16}$$

Using the Euler backward implicit integration scheme, the trial stress is modified under consideration of the occurring plastic strains as long as convergence is reached. The

convergence criterion is fulfilled when the iterative stress state returns to the yield surface ($f_y < 10^{-7}$). If the plasticity is associated with a given strain increment, it is essential to calculate the following system of equations

$$\boldsymbol{\sigma}'_{n+1} = \boldsymbol{\sigma}'_{n} + d\boldsymbol{\sigma}' \tag{17}$$

By using the plastic multiplier in Eq. (13), given the strain increment is applied to arrive at the elastic predictor, the stress increment $d\boldsymbol{\sigma}'$ can be calculated as

$$d\boldsymbol{\sigma}' = \boldsymbol{D}_e d\boldsymbol{\varepsilon} - d\Lambda \boldsymbol{D}_e \frac{\partial f_y}{\partial \boldsymbol{\sigma}'} \tag{18}$$

In this implementation, size of load (strain) increment is controlled by sub-stepping within the subroutine in order to obtain solutions. Maximum strain increment used to simulate the results presented in this paper is $|d\boldsymbol{\varepsilon}| < 0.1\%$. Figure 4 presents a summary of the Euler backward algorithm to implement the proposed model.

4. Model features

4.1 Slope and uniqueness of the CSL

The strength at the ultimate state after large strains have developed, i.e. at critical state, is controlled by the plastic potential surface. For isotropic contractancy models, the slope of the critical state line (CSL) is equal to M (e.g. [18]). However, for anisotropic contractancy models, the slope of the CSL in stress space (p' - q) is not usually M (e.g. Extended Sekiguchi-Ohta models [16]) and it depends on both M and n_L. The E-SCLAY1S model has been developed to preserve M as the slope of the CSL in stress space, which is a main advantage with respect to the Extended Sekigucha-Ohta models. The slope of the CSL is demonstrated in the following.

At critical state condition, there are no plastic volumetric strains, so

$$\frac{\partial f_y}{\partial p'} = 0 \tag{18}$$

Differentiating Eq. (2)

$$\frac{\partial f_y}{\partial p'} = \left(1 + \frac{|\eta - \alpha|^{n_L}}{M^{n_L} - \alpha^{n_L}}\right)^{\Psi} - \frac{\Psi n_L \eta |\eta - \alpha|^{n_L - 1}}{M^{n_L} - \alpha^{n_L}} \left(1 + \frac{|\eta - \alpha|^{n_L}}{M^{n_L} - \alpha^{n_L}}\right)^{\Psi - 1} \tag{19}$$

and rearranging terms in Eq. (19)

$$\frac{\partial f_y}{\partial p'} = \left(1 + \frac{|\eta - \alpha|^{n_L}}{M^{n_L} - \alpha^{n_L}}\right)^{\Psi - 1} \frac{1}{M^{n_L} - \alpha^{n_L}} \left(M^{n_L} - \alpha^{n_L} + |\eta - \alpha|^{n_L} - \Psi n_L \eta |\eta - \alpha|^{n_L - 1}\right) \tag{20}$$

the slope of the CSL is given by η

$$M^{n_L} - \alpha^{n_L} + |\eta - \alpha|^{n_L} - \Psi n_L \eta |\eta - \alpha|^{n_L - 1} = 0 \tag{21}$$

Eq. (21) may be developed substituting the value of Ψ (Eq. 3).

$$\frac{M^{n_L} - \alpha^{n_L} + |\eta - \alpha|^{n_L}}{M^{n_L} - \alpha^{n_L} + (M - \alpha)^{n_L}} = \frac{\eta}{M} \frac{|\eta - \alpha|^{n_L - 1}}{(M - \alpha)^{n_L - 1}} \tag{22}$$

From Eq. (22), it is clear that the slope of the CSL for triaxial compression is $\eta = M$. For triaxial extension, the slope of the CSL seems to depend not only on M but also on n_L, see for example the shape of the yield surface in p' - q plots (Figure 2). However, for triaxial extension, the yield surface rotates towards the extension side, and at critical state, the inclination of the yield surface (α) is on the extension side, i.e. α is negative, and Eq. (22) gives the same result for extension and for compression ($\eta = M$). Only for the unrealistic case of initial fabric anisotropy but without evolution of that fabric during plastic straining, i.e. deactivating the rotational hardening rule, the CSL would be different for compression and triaxial extension depending on n_L in stress space:

- higher than M for $n_L<2$
- equal to M for $n_L=2$
- lower than M for $n_L>2$

The constant slope of the CSL in stress space for any value of n_L, if rotational hardening is allowed, is also valid for any other direction in the π–plane, i.e. for any Lode's angle. In the current implementation of the model, no attempt has been made to distinguish between compression and extension, i.e. $M_c=M_e$, or include any dependency on Lode's angle, so it corresponds to the Drucker-Prager criterion (see Figure 3).

The E-SCLAY1 model also preserves the uniqueness of the CSL as illustrated in Figure 5, where the solid lines with arrows on p'-axis show the uniqueness of the CSL in stress space. To highlight and confirm the uniqueness of the CSL in stress space, undrained triaxial compression and extension tests were simulated from a K_0 consolidated state (Figure 6). The rotation of the initial yield surface to the extension side during triaxial extension tests leads to the same slope both in compression and in extension, which is equal to M (Figure 6a). If the yield surface is not allowed to rotate, i.e. no rotational hardening ($\omega=0$), the slope of the CSL at extension depends on the n_L value as previously mentioned (Figure 6b). However, this is a very unrealistic case, which should not be modelled and has been presented only for illustrative purposes.

The rotational hardening rule of the S-CLAY1 model was developed to predict a unique CSL in the e-ln p' space. In the case of the proposed E-SCLAY1S model, the uniqueness of the CSL in the e-ln p' space is preserved for a given n_L value too. The

vertical separation from the isotropic normal compression line (NCL) to the CSL in the e-ln p' space predicted by the E-SCLAY1S model is given by

$$e_N - e_\Gamma = (\lambda_i - \kappa)\left(\frac{\ln\left(1 + \frac{(M - \chi_d(M))^{n_L}}{M^{n_L} - \chi_d(M)^{n_L}}\right)\left(M^{n_L} - \chi_d(M)^{n_L} + (M - \chi_d(M))^{n_L}\right)}{n_L M (M - \chi_d(M))^{n_L - 1}} \right) \quad (23)$$

where e_N is the void ratio on the NCL that corresponds to a unit stress and e_Γ is the void ratio of the CSL at a unit stress. $\chi_d(M)$ is the predicted unique inclination of the yield curve at critical states, which is equal to $M/3$ [9].

For n_L=2 (S-CLAY1), the above equation reduces to equation (6) of Wheeler et al. [9], and for n_L=2 and α=0 (MCC) the above equation reduces to $e_N - e_\Gamma = (\lambda - \kappa)\ln 2$. The normalized vertical separation $\left(\frac{e_N - e_\Gamma}{\lambda_i - \kappa}\right)$ to the NCL in the e-ln p' space at critical state with the n_L value is presented in Figure 7. For comparison, (original) Cam Clay (CC), modified Cam Clay (MCC) and S-CLAY1 are also presented in the figure. It can be seen that the proposed model has flexibility in predicting the CSL in the e-ln p' space compared to the previously developed models. According to Wheeler et al. [9], the experimental data from tests on Otaniemi clay do not provide evidence for a unique CSL in the e-ln p' space.

4.2 K_0 prediction

The (original) CC model clearly overpredicts the coefficient of lateral earth pressure at rest for normally consolidation conditions, K_{0NC} [24]. Although the MCC model predicts more realistic values than the (original) CC model, it is well known to still overpredict K_{0NC} (e.g. [24]). Therefore, some authors (e.g. Federico et al. [25]) have used plastic potential surfaces with higher degrees of freedom to fit the desired K_{0NC} value. Federico

et al. [25] also present a wide analysis of the analytical expressions that give K_{0NC} for isotropic critical state models. The analytical expression that gives the value of K_{0NC} for E-SCLAY1S is derived in Appendix II. The variation of the K_{0NC} stress path with n_L is illustrated in Figure 8 for an initially isotropically consolidated soil sample.

The isotropic version of E-SCLAY1 (α=ω=0) is a hierarchical extension of MCC that introduces the additional parameter n_L, which may be correlated with K_{0NC} using Eq. (II.7). The variation of K_{0NC} with n_L is shown in Figure 9a. Although a perfect fit of n_L could be applied for each case, a value of n_L around 3.5 gives similar values to those of Jaky's empirical formula (K_{0NC}=1-sin ϕ). However, the yield function for that value (n_L=3.5) could lead to unrealistic high undrained shear strengths (Figure 9b). To avoid that, a non-associated flow rule could be proposed, using a n_L value lower than 2 for the yield surface (e.g. 1.3) and a high n_L value (e.g. 3.5) for the plastic potential surface. Nevertheless, the isotropic version of E-SCLAY1 has been presented to show its similar capabilities to other previous studies (e.g. [25]), but, even initially remoulded soils show some fabric under one dimensional compression (e.g. [26,27]), and the authors believe that trying to fit K_{0NC} values with isotropic plastic potential surfaces is not realistic.

Once soil anisotropy is introduced, the proper K_{0NC} can be fitted adjusting the inclination of the yield surface, α_0 (e.g. [9]), because it is difficult to have enough accurate data to determine the initial inclination of the yield surface (α_0) and this inclination seems to be related to one dimensional compression of the soil during its deposition through K_{0NC}. The E-SCLAY1 model, through the n_L parameter, introduces more flexibility in the possibilities to fit K_{0NC} and the initial inclination of the yield surface (α_0). However, in practical situations, there are not enough data about the initial

inclination of the yield surface and the practical approach here proposed is to fit all the parameters similarly to S-CLAY1 [9] and the additional parameter of the E-SCLAY1 model (n_L), using the undrained shear strength.

4.3 Undrained shear strength

One of the most important risks associated with the numerical simulation of geotechnical engineering problems under undrained conditions using soil constitutive models formulated in effective stresses is the possible unrealistic prediction of the undrained shear strength. That occurred, for example, in the numerical simulation of the deep excavation near the Nicoll Highway, Singapore that collapsed in 2004 (Whittle and Davies [28]). The additional parameter (n_L) of the E-SCLAY1 model allows for a perfect matching of the undrained shear strength (c_u) as it will be shown in the comparison with laboratory measurements in Section 5. The variation of c_u with n_L may be seen in Figure 6a.

For an initially isotropically and normally consolidated soil sample, c_u may be normalized by the initial mean effective pressure, p'_0. Figure 10 shows the predicted values by the isotropic version of E-SCLAY1 model depending on n_L. For the sake of simplicity, the isotropic version of E-SCLAY1 is used. Then, it may be demonstrated that $\frac{c_u}{p'_0} = \frac{M}{2^{\frac{2}{n_L}\left(1-\frac{\kappa}{\lambda}\right)+1}}$

4.4 Yield loci

The E-SCLAY1 model, through the n_L parameter, provides an additional flexibility in comparison with the conventional S-CLAY1 model to fit the initial yield surface.

However, in practical situations there is little information about the initial yield surface and even for the well-documented cases, there are some problems associated with its determination, for example regarding the homogeneity of the natural soil samples and the identification of soil yielding (e.g. [27]).

Most published yield loci (e.g. McGinty [29]) have been determined using bilinear interpretation of *e*-ln *p'*. This methodology is similar to the Casagrande method used to calculate the preconsolidation pressure and is summarized, for example in Graham et al. [30]. The methodology involves some ambiguity because the behavior of clay is non-linear except at very small strains and some engineering judgment is necessary. Besides, for soils with evolving anisotropy and different loading stress ratios, the methodology is not appropriate (e.g. McGinty [29]). For loading stress ratios that deviate from the initial loading stress ratio, yield curve rotation starts to develop under small volumetric strains before the strains get larger due to isotropic hardening. Consequently, the bilinear interpretation of *e*-ln *p'* curves tend to overestimate yield stresses for stress paths that notably deviate from the initial one (e.g. Figure 11). To overcome these limitations, arithmetic stress scale (e.g. *e-p'*) is generally used (e.g. [27,31]).

Being aware of the limitations of most published yield loci and as an example of the improved capabilities of the E-SCLAY1 model, the yield surfaces of some well-documented soils are fitted in Figure 12. The initial inclination of the yield surface was determined as proposed by Wheeler et al. [9] based on M, i.e. K_{0NC} determined using Jaky's expression. The experimental data are taken from Graham et al. [32], Wheeler et al. [9] and Díaz-Rodríguez et al. [33]. No attempt to get the best fit was made, and only for illustration, the yield surfaces using n_L=2.5, which match better the experimental

data than those using n_L=2.0, are presented in Figure 12. The size of the yield surface, p'_m, was kept constant.

4.5 Soil deformation

For normally consolidated conditions under constant stress ratios (η), the parameter λ controls compressive volumetric strains because E-SCLAY1 is as a Cam Clay model. For shearing stress paths, compressive volumetric strains depend on the additional contractancy parameter (n_L). As an illustrative example, Figure 13a shows the results of simulated drained triaxial compression tests for different n_L values. The soil response is stiffer for higher n_L values. The influence of n_L on the soil stiffness during shearing is summarized in Figure 13b, using the E_{50}/E_{oed} ratio, where E_{50} is the secant Young's modulus at 50% of the failure load in a conventional drained triaxial test at a given cell pressure (p_{ref}) and E_{oed} is the tangent Young's modulus for confined compression at the same pressure (p_{ref}), which does not depend on n_L ($E_{oed} = p_{ref}(1+e)/\lambda$).

A higher n_L value reduces the space between the NCL and the CSL (Eq. 23 and Figure 7) and, therefore, the soil response is stiffer for shearing stress paths. The proposed model (E-SCLAY1S) is a logarithmic contractancy model [18], which means that uses a logarithmic description of the compressive volumetric strains, ε_v, during drained shear at constant mean effective stress and normally consolidated conditions (Eqs. I.1 and I.4). So, n_L controls the volumetric strains during shearing and its variation with the stress ratio, η. Ideally, n_L could be calibrated by fitting experimental laboratory results of drained triaxial shear tests at constant mean effective stress. The influence of n_L in the contractancy results is shown in Figure 14. Volumetric strains (ε_v) are normalized by the volumetric strain at critical state (ε_{vM}) and the stress ratio (η) is normalized by the stress

ratio at critical state (M) to isolate the influence of n_L from other model parameters. As an example, laboratory data on isotropically consolidated remolded kaolin clay by Hattab and Hicher [34] are also presented in Figure 14.

4.6 Destructuration

For the sake of completeness, the model has been formulated including soil structure and loss of bonding. This model feature performs similarly to that of the S-CLAY1S model [12], so it has not been considered necessary to include here any specific simulation or comment about it.

5. Comparison with experimental data

In this section, the proposed model (E-SCLAY1S) is validated against some laboratory results published in the literature. As some of the capabilities of the proposed model are similar to those of the well-studied S-CLAY1S model, the focus here is on the improvement provided by the additional contractancy parameter (n_L). All the parameters of the model but n_L coincide with the S-CLAY1S model, so the approach proposed by Wheeler et al. [9], which gives satisfactory results for most cases (e.g. [12-15]), is here used to determine those parameters. The additional parameter n_L has been vary to get a better fit of the experimental results, usually, of the undrained shear strength.

5.1 Kaolin clay

Stipho [26] conducted a series of undrained triaxial tests on isotropically and anisotropically consolidated specimens of Kaolin clay. Several degrees of overconsolidation (from 1 to 4 or 12) and initial anisotropy (K_0 ranging from 1 to

K_{0NC}=0.57) were used. The tests were stress controlled and consequently, failure may not have been properly captured. Several researchers have used the results for verifying their constitutive models (e.g. [35,36]). The parameters used in the numerical simulations are summarized in Table 1. They have been directly taken either from previous studies [35,36] for standard critical state parameters or following Wheeler et al. [9] for anisotropy. The parameter that controls the rotation of the yield surface with the plastic strains, ω, was set equal to a very low value (0.5), typical for remolded Kaolin clay. Only the contractancy parameter was fitted to get a better agreement with the experimental results, particularly with c_u. The best fit of n_L is compared with S-CLAY1 (n_L=2) in Figure 15. For isotropically consolidated samples, the agreement is very good for n_L=1.3. In addition to stress paths, the stress-strain curves and the generated pore pressures are also well predicted by the model (Figure 16).

For anisotropically consolidated samples (K_0<1), it was necessary to gradually increase the value of n_L to get a good matching of the experimental results (Figure 15). For normally consolidated samples at K_0=0.67 and 0.57, the matching was not possible and by observing the stress paths, it can be deduced that the waiting times after consolidation could have slightly overconsolidated the soil samples due to aging or creep effects. A good agreement was found for S-CLAY1 (n_L=2), using the best fit value of OCR due to aging (1.1 for K_0=0.67 and 1.2 for K_0=0.57). For the sake of comparison, the stress paths for OCR=1 are also included in Figure 15 and the starting points are the same because the applied initial stresses were p'/p'_0=1.

The initial rotation of the yield surface (α_0) for anisotropically consolidated samples was obtained by simulation of the K_0 stress paths with n_L=2. The proposed model (E-

SCLAY1) is an extension of S-CLAY1 and, therefore, it shares some of the limitations, such as a good behaviour only for normally or slightly overconsolidated soft soils. For high degrees of overconsolidation, the flexibility introduced by n_L improves the numerical predictions only for isotropically consolidated samples.

5.2 Santa Clara clay

Venda Oliveira and Lemos [27] present laboratory results of a sandy lean clay from Santa Clara dam area, Portugal. The clay was reconstituted prior to testing. They performed triaxial tests on isotropically and K_0 consolidated clay samples to evaluate several elastoplastic models. Stress path controlled drained triaxial tests were performed to determine the position of the initial yield surface and the direction of plastic strain increments ($d\varepsilon^p$). The specimens used to study the isotropic behavior were initially normally consolidated to an isotropic effective stress (p'_m) of 200 kPa and subsequently unloaded and consolidated to an effective isotropic pressure of 100 kPa, which resulted in an OCR (p'_m/p') of 2.0. Four drained triaxial tests with stress paths, dq/dp', equal to 1.0, 2.5, 3.0 and 5.0 were then performed (Figure 17).

The specimens used to analyze the anisotropic behavior were initially subjected to K_0 consolidation (K_0=0.47) to reach a normally consolidated state of a vertical effective stress of σ'_{vc}=200 kPa (σ'_{hc}=94 kPa). Then, the specimens were unloaded and consolidated to a vertical effective stress of σ'_{v0}=160 kPa (σ'_{h0}=80 kPa), corresponding to an OCR ($\sigma'_{vc}/\sigma'_{v0}$) of 1.25. Four drained triaxial tests with stress paths, dq/dp', equal to -1.5, -0.5, 1.0 and 3.0 were then performed (Figure 18).

Careful evaluation of the yield loci based on both ε_1–p' and ε_v-p' plots was performed and the probable limits of the yield zone are provided (inverted triangles). They also performed undrained compression triaxial tests to evaluate undrained stress paths (blue crosses) under normally consolidated conditions.

Using the proposed model (E-SCLAY1), the results of those undrained compression triaxial tests were numerically simulated. The soil parameters for the numerical model are shown in Table 1 and were directly taken from [27]. Figure 17 compares the laboratory results with the numerical predictions for the isotropically consolidated Santa Clara clay. For the numerical simulations, two n_L values, namely n_L=2 (S-CLAY1) and n_L=1.3 (best-fit value) were used. Although the undrained stress path measured in the laboratory (blue crosses) is slightly irregular at the beginning, the best fit value (n_L=1.3) provides a good match of the laboratory results and notably improves the results for n_L=2. The initial yield surfaces of the model for n_L=1.3 ("bullet" shape) and 2 (elliptical) are also shown for evaluation against the yield zone (inverted triangles) and plastic strain increments (arrows). The soil exhibits some rotational hardening (ω=200 and ω_d=0.91), which causes some deviation of the numerically simulated undrained stress paths from the initial yield surfaces. The agreement between the limits of the yield zone and the initial yield surface for n_L=1.3 is not as good as for the undrained stress path, which may be explained by the difficulties associated with the determination of yield loci.

Figure 18 compares the results for the K_0 consolidated Santa Clara clay. In this case, it is difficult to get a good fit of the experimental undrained stress path (blue crosses), and the best fit value (n_L=1.8) was determined to match the undrained shear strength. As for

the Kaolin clay, it was necessary to use a different n_L value (1.8) than that of the isotropic case (1.3). For anisotropic conditions, the differences with S-CLAY1 (n_L=2) are not very important. As for the initially isotropic case, the initial yield surfaces of the model are also shown for evaluation against the yield zone and plastic strain increments. Plastic strain increments are plotted in (Figures 17-18) for completion, but it is worth noting that plastic strain vectors are difficult to determine in practice because it is necessary to assume an elastic law and the strain increments need to be small but at the same time large enough to eliminate noises in the measurements.

6. Discussion on the shape of the yield surface

The contractancy parameter (n_L) controls the shape of the yield surface, yet, in practical situations, n_L may be conveniently calibrated to fit c_u or the stiffness along shearing paths. From the comparison with experimental results (Figures 15-18), it seems that the n_L value may not be constant and may depend on the degree of anisotropy because for isotropically consolidated soils, its value is around 1.3, while for anisotropic conditions it is close to n_L=2, which corresponds to S-CLAY1. Although there may be some uncertainties related to the quality of the experimental data, the shape of the yield function for isotropic conditions seems to be closer to the original Cam Clay model than to the Modified Cam Clay model, while for anisotropic conditions a rotated and distorted yield surface seems appropriate (e.g. S-CLAY1). As an additional example, Figure 19 shows experimental values of yield stresses for Bothknennar clay (data after McGinty [29]). For intact soil samples (Figure 19a), the yield surface of the S-CLAY1 model fitted through the experimental data points using M=1.4 and α_{K0}=0.31 (after McGinty [29]). The size of the yield surface (p'_m=85 kPa) was obtained by McGinty [29] optimizing the best fit to the experimental data. As explained in Section 4.4, the

yield points (black dots) have been determined using bilinear interpretation of *e*-ln *p'* curves and this may lead to an overestimation of the yield stress for those stress paths that cause significant rotation of the yield surface, e.g. triaxial extension for this case. Consequently, a good fitting of the yield points for triaxial extension could only be possible introducing a different slope of the CSL for extension (M_e) i.e. introducing a Lode's angle dependent failure criterion.

McGinty [29] also checked the yielding points of Bothkennar clay after isotropic consolidation (Figure 19b). The single square point indicates the maximum stress in the common first loading stage (210 kPa), while circular points represent yield points identified from individual second loading stages. The yield points in Figure 19b are reasonably symmetric about the *p'*-axis, suggesting that, as expected, the isotropic loading in the first stage had rotated the yield curve clockwise to an isotropic orientation i.e. symmetrical about the *p'*-axis. To improve the accuracy of the yield points, the authors have reinterpreted McGinty [29] data using arithmetic stress scale and volumetric and axial engineering strains (Figure 20). Only compression tests and isotropically consolidated samples have been reinterpreted because those are particularly relevant for the comparison here presented about the shape of the yield surface. In the reinterpretation, instead of a yield point, a yield zone has been identified. This yield zone has been included in Figure 19b as a line between crosses. In most tests, an initial non-linear stress-strain behaviour is observed for low stresses. After that, a linear part may be identified, and later, the data show the initiation of an exponential curve, which marks the yield stress (see Figure 20). The linear part has been fitted by a straight line (dashed) to precisely identify the initiation of the exponential behaviour. A yield zone was chosen, as the results for volumetric and axial strains seem to be slightly

different. Although McGinty [29] yield points tend to generally underestimate the yield stress, e.g. for isotropic consolidation (Figure 19b), the reinterpretation confirms that the yield stress is overestimated for stress paths that notably differ from the initial one, if a logarithmic stress scale is used, e.g. for η_2=1.3.

The yield curve expression for S-CLAY1 (n_L=2) with α_{K0}=0.0 and p'_m=210 kPa (corresponding to the Modified Cam Clay yield curve expression) is a poor match to the experimental data (Figure 19b). The E-SCLAY1S model using n_L=1.4 gives a good matching of the experimental data and confirms the differences in the shape of the yield surface between anisotropic and isotropic consolidated samples. The experimental yield points in extension give lower values that those predicted by the model as expected, because no dependency on the Lode's angle has been introduced in the model.

Conclusions

An anisotropic model for structured clays (E-SCLAY1S) has been formulated to extend a previous model (S-CLAY1S [12]) for normally or slightly overconsolidated soft clays by introducing the framework of logarithmic contractancy.

In addition to a complete description of the proposed model in triaxial stress space, an implicit Euler backward algorithm for the stress integration has been presented. A major advantage of this framework is that by suitable adjustment of the parameter (n_L) a wide range of yield surface shapes can be achieved. It is important to acknowledge the fact that the proposed model requires only an additional parameter (n_L) and it can be determined from conventional laboratory tests (drained or undrained triaxial tests). As compared to the non-associated flow rule presented by Dafalias and Taiebat [19] for

improved predictions, the present model has the advantage of being simpler to calibrate and to implement into a finite element code.

The main features of the model can be summarized as follows:

1. Uniqueness of the critical state line (CSL) at stress space and constant slope of CSL as M, independently of n_L value - this is a major advantage of the proposed model compared to previous anisotropic logarithmic contractancy models (e.g. Extended Sekiguchi-Ohta models [16]).
2. K_0 prediction and yield loci – the proposed model through the additional parameter (n_L) introduces more flexibility in predicting K_0 and the yield points in p'-q space.
3. Undrained shear strength (c_u) – an improved prediction of c_u can be obtained by adjusting the logarithmic contractancy parameter n_L.
4. Stiffness– the additional parameter (n_L) may be also used to fit the stiffness under shearing stress paths.

The comparisons with laboratory test data of two remoulded clays for different stress and overconsolidation ratios under undrained shearing revealed the predictive capabilities of the proposed model. The experimental data on Bothkennar clay, Santa Clara clay and Kaolin clay suggest that the model parameter n_L, which controls the shape of the yield surface, may not be a soil constant and it can be a hardening parameter that varies with the amount of fabric (degree of anisotropy) of clays. However, further experimental studies on yield points are required to conclude that the parameter n_L varies with the degree of anisotropy.

The model verification is limited to soils that do not exhibit bonding and destructuration behaviour with plastic straining. Since triaxial tests were used for validation, additional work should be conducted to verify the model for other stress paths, and also in boundary value problems. Further extension of the model to account for rate-dependent (creep) natural soft soil response can be made along the lines presented by Sivasithamparam et al. [37].

Acknowledgements

The research was carried out as part of GEO-INSTALL (Modelling Installation Effects in Geotechnical Engineering, PIAP-GA-2009-230638) project supported by the European Community through the programme Marie Curie Industry-Academia Partnerships and Pathways (IAPP) under the 7th Framework Programme. The authors would like to acknowledge the valuable suggestions and insights offered by Prof. Minna Karstunen at Chalmers University of Technology, Sweden & Department of Civil Engineering, University of Strathclyde, Glasgow, UK.

References

[1] Roscoe KH, Schofield AN, Wroth CP. On the yielding of soils. Géotechnique 1958; 8(1): 22–53.

[2] Roscoe KH, Schofield AN. Mechanical behaviour of an idealised ‘wet’ clay. Proc Eur Conf Soil Mech Found Eng, Wiesbaden;1963. Vol. 1. p. 47-54.

[3] Schofield AN, Wroth CP. Critical State Soil Mechanics. London: McGraw-Hill; 1968.

[4] Roscoe KH, Burland JB. On the generalised stress-strain behaviour of 'wet' clay. In Engineering Plasticity (Heyman J, Leckie FA, eds), p. 563-609. Cambridge: Cambridge University Press; 1968.

[5] Kim MK, Lade PV. Single hardening constitutive model for frictional materials. I. Plastic potential function. Comput Geotech 1988; 5: 307–24.

[6] Lade PV, Kim MK. Single hardening constitutive model for frictional materials. II. Yield criterion and plastic work contours. Comput Geotech 1988; 6: 13–29.

[7] Lagioia R, Puzrin AM, Potts DM. A new versatile expression for yield and plastic potential surfaces. Comput Geotech 1996; 19(3): 171–91.

[8] Dafalias YF. An anisotropic critical state soil plasticity model. Mechanical Research Communications 1986; 13(6): 341–47.

[9] Wheeler SJ, Naatanen A, Karstunen K, Lojander M. An anisotropic elastoplastic model for soft clays. Can Geotech J 2003; 40(2): 403–18.

[10] Whittle AJ, Kavvadas, MJ. Formulation of MIT-E3 constitutive model for overconsolidated clays. J. Geotech Eng, ASCE 1994; 120(10): 173–98.

[11] Sekiguchi H, Ohta H. Induced anisotropy and time dependency in clays. Proc specialty session 9, Constitutive equation of soils, 9th Int Conf Soil Mech Found Eng 1977; Tokyo, p. 306–15.

[12] Karstunen M, Krenn H, Wheeler SJ, Koskinen M, Zentar, R. Effect of anisotropy and destructuration on the behaviour of Murro test embankment. Int J Geomech 2005; 5(2): 87–97.

[13] Karstunen M, Wiltafsky C. Krenn H, Scharinger F, Schweiger HF. Modelling the behaviour of an embankment on soft clay with different constitutive models. Int J Numer Anal Methods Geomech 2006; 30: 953–82.

[14] Karstunen M, Koskinen M. Plastic anisotropy of soft reconstituted clays. Can Geotech J 2008; 45(3): 314–28.

[15] Yildiz A, Karstunen M, Krenn H. Effect of anisotropy and destructuration on behavior of Haarajoki test embankment. Int J Geomech 2009; 9: 153–68.

[16] Ohta H, Iizuka A, Ohno S. Constitutive modelling for soft cohesive soils. In Geotechnics and Earthquake Geotechnics Towards Global Sustainability (Iai S, ed), Chapter 13, p. 231–50. Springer: Dordrecht, 2011.

[17] Shibata T. On the volume changes of normally consolidated clays. Disaster Prevention Research Institute Annuals, Kyoto Univeristy, Vol. 6, p. 128-34; 1963 (In Japanese).

[18] Ohno S, Iizuka A, Ohta H. Two categories of new constitutive model derived from non-linear description of soil contractancy. J Appl Mech, JSCE 2006; 9: 407–14 (in Japanese).

[19] Dafalias YF, Taiebat, M. Anatomy of rotational hardening in clay plasticity. Geotechnique 2013; 63(16): 1406–18.

[20] Gens A, Nova R. Conceptual bases for a constitutive model for bonded soils and weak rocks. In Geomechanical engineering of hard soils and soft rocks (Anagnostopoulos A, Schlosser F, Kaltesiotis N, Frank R, eds). A.A. Balkema: Rotterdam, 1993. Vol. 1, p. 485–94.

[21] Whittle AJ, DeGroot DJ, Ladd CC, Seah TH. Model prediction of anisotropic behaviour of Boston Blue Clay. J Geotech Eng, ASCE 1994; 120(1): 199–224.

[22] Sivasithamparam, N. Development and implementation of advanced soft soil models in finite elements. PhD thesis, University of Strathlcyde, Glasgow; 2012.

[23] Brinkgreve RBJ, Engin E, Swolfs WM. Plaxis 2D 2012 Manual. Plaxis bv, the Netherlands; 2012.

[24] Potts DM, Zdravkovic L. Finite element analysis in geotechnical engineering: theory. Thomas Telford: London, 1999.

[25] Federico A, Elia G, Murianni, A. The at-rest earth pressure coefficient prediction using simple elasto-plastic constitutive models. Comput Geotech 2009; 36(1-2): 187–98.

[26] Stipho AS. Theoretical and experimental investigation of the behavior of anisotropically consolidated Kaolin. PhD thesis, University College, Cardiff; 1978.

[27] Venda Oliveira PJ, Lemos LJL. Experimental study of isotropic and anisotropic constitutive models. J Geotech Eng, ASCE 2014; 140 (8): 06014008:1-7.

[28] Whittle AJ, Davies RV. Nicoll Highway Collapse: Evaluation of geotechnical factors affecting design of excavation support system. International Conference on Deep Excavations, 28-30 June 2006, Singapore.

[29] McGinty, K. The stress-strain behaviour of Bothkennar clay. Ph.D. thesis, Department of Civil Engineering, University of Glasgow; 2006.

[30] Graham J, Crooks JHA, Lau SLK. Yield envelopes: identification and geometric properties. Geotechnique 1988; 38(1): 125–34.

[31] Graham J. The 2003 R.M. Hardy lecture: Soil parameters for numerical analysis in clay. Can Geotech J 2003; 43(2): 187–209.

[32] Graham J, Noonan ML, Lew KV. Yield states and stress-strain relations in natural plastic clay. Can Geotech J 1983; 20: 502–16.

[33] Diaz-Rodriguez JA, Leroueil S, Aleman JD. Yielding of Mexico City clay and other natural clays. J Geotech Eng, ASCE 1992; 118(7): 981–95.

[34] Hattab M, Hicher P-Y. Dilating behaviour of overconsolidated clay. Soils Found 2004; 44(4): 27–40

[35] Banerjee PK, Yousif NB. 1986. A plasticity model for the mechanical behavior of anisotropically consolidated clay. Int J Numer Analyt Meth Geomech 1986; 10: 521–41.

[36] Ling HI, Yue D, Kaliakin VN, Themelis, NJ. Anisotropic Elastoplastic Bounding Surface Model for Cohesive Soils. J Eng Mech 2002; 128: 748–58.

[37] Sivasithamparam N, Karstunen M, Bonnier P. Modelling creep behaviour of anisotropic soft soils. Comput Geotech 2015; 69: 46-57.

APPENDIX I: Yield surface

In the general contractancy framework proposed by Ohno et al. [18], the negative strains (contractancy) developed during drained triaxial tests at constant mean stress (p') may be fitted by a general function H:

$$e = e_0 - (e_0 - e_M)H \tag{I.1}$$

where e_0 is the initial void ratio after isotropic loading and e_M is the void ratio at critical state. H is a function of the stress ratio η ($=q/p'$) and indicates the relative position of any of the parallel lines between the NCL and the CSL. Following the development by Ohta et al. [16], the yield function may be found as

$$f_y = \frac{\lambda_i - \kappa}{1 + e_0} \ln \frac{p'}{p'_m} + \varepsilon_{vM} H = 0 \tag{I.2}$$

Where ε_{vM} is the volumetric strain at critical state and may be demonstrated to be

$$\varepsilon_{vM} = -\frac{\dfrac{\lambda_i - \kappa}{1 + e_0}}{p' \dfrac{\partial H}{\partial p'}} \tag{I.3}$$

when $|\eta| = M$ (critical state).

Here, the following logarithmic contractancy function is proposed

$$H = \frac{\ln\left(1 + \dfrac{|\eta - \alpha|^{n_L}}{M^{n_L} - \alpha^{n_L}}\right)}{\ln\left(1 + \dfrac{(M - \alpha)^{n_L}}{M^{n_L} - \alpha^{n_L}}\right)} \tag{I.4}$$

The value of H=0 for isotropic loading (where η=0 and α=0) and the value of H=1 for the CSL (e.g. triaxial compression, where η=M).

Differentiating H with respect to p' and substituting for critical state conditions (η=M)

$$\frac{\partial H}{\partial p'}\,p' = -\frac{1}{\ln\left(1+\dfrac{(M-\alpha)^{n_L}}{M^{n_L}-\alpha^{n_L}}\right)}\,\frac{n_L M(M-\alpha)^{n_L-1}}{M^{n_L}-\alpha^{n_L}+(M-\alpha)^{n_L}} \tag{I.5}$$

the yield function is obtained using Eq. (I.3), (I.4) and (I.5)

$$f_y = \ln\left(\frac{p'}{p'_m}\right) + \Psi \ln\left(1+\frac{|\eta-\alpha|^{n_L}}{M^{n_L}-\alpha^{n_L}}\right) = 0 \tag{I.6}$$

where, for the sake of brevity, Ψ is the following constant

$$\Psi = \frac{M^{n_L}-\alpha^{n_L}+(M-\alpha)^{n_L}}{n_L M(M-\alpha)^{n_L-1}} = \frac{(M-\alpha)}{n_L M}\left[1+\frac{M^{n_L}-\alpha^{n_L}}{(M-\alpha)^{n_L}}\right] \tag{I.7}$$

Combining the logarithms in Eq. (I.6)

$$f_y = \ln\left[\frac{p'}{p'_m}\left(1+\frac{|\eta-\alpha|^{n_L}}{M^{n_L}-\alpha^{n_L}}\right)^{\Psi}\right] = 0 \tag{I.8}$$

and eliminating the logarithm, the yield function may be expressed as

$$f_y = \left(1+\frac{|\eta-\alpha|^{n_L}}{M^{n_L}-\alpha^{n_L}}\right)^{\Psi} - \frac{p'_m}{p'} = 0 \tag{I.8}$$

APPENDIX II: K_0 value

The proposed model (E-SCLAY1S) allows for an analytical derivation of the K_0 value as presented below.

The rates of shear and volumetric plastic strains are related by the associated flow rule:

$$\frac{\dot{\varepsilon}_q^p}{\dot{\varepsilon}_v^p} = \frac{\partial f_y \big/ \partial q}{\partial f_y \big/ \partial p'} \tag{II.1}$$

The plastic potential surface is given by Eq. (2), which may be rearranged to give

$$f_y = p'\left(1+\frac{|\eta-\alpha|^{n_L}}{M^{n_L}-\alpha^{n_L}}\right)^{\Psi} - p'_m = 0 \tag{II.2}$$

Differentiating Eq. (II.2) with q

$$\frac{\partial f_y}{\partial q} = \frac{\Psi n_L |\eta-\alpha|^{n_L-1}}{M^{n_L}-\alpha^{n_L}}\left(1+\frac{|\eta-\alpha|^{n_L}}{M^{n_L}-\alpha^{n_L}}\right)^{\Psi-1} \tag{II.3}$$

and differentiating Eq. (II.2) with p' (Eq. 20), the quotient between Eq. (II.3) and Eq. (20) gives the slope of the associated flow rule

$$\frac{\partial f_y/\partial q}{\partial f_y/\partial p'} = \frac{\Psi n_L |\eta-\alpha|^{n_L-1}}{\left(M^{n_L}-\alpha^{n_L}+|\eta-\alpha|^{n_L}-\Psi n_L \eta|\eta-\alpha|^{n_L-1}\right)} \tag{II.4}$$

Under confined one dimensional consolidation (K_0 consolidation), the rate of horizontal strains is null and then

$$\frac{\dot{\varepsilon}_q}{\dot{\varepsilon}_v} = \frac{2}{3} \tag{II.5}$$

Assuming that the elastic strains are much smaller than the plastic strains, Eq. (II.5) may be approximate by

$$\frac{\dot{\varepsilon}_q^p}{\dot{\varepsilon}_v^p} = \frac{2}{3} \tag{II.6}$$

Substituting Eq. (II.4) into Eq. (II.1), and then into Eq. (II.6), the equation that implicitly gives η_{K0} is obtained

$$\frac{\Psi n_L |\eta_{K0}-\alpha|^{n_L-1}}{\left(M^{n_L}-\alpha^{n_L}+|\eta_{K0}-\alpha|^{n_L}-\Psi n_L \eta_{K0}|\eta_{K0}-\alpha|^{n_L-1}\right)} = \frac{2}{3} \tag{II.7}$$

K_0 may be obtained from η_{K0}

$$K_0 = \frac{3-\eta_{K0}}{3+2\eta_{K0}} \tag{II.8}$$

For n_L=2 (Ψ=1), Eq. (II.7) reduces to equation (13) of Wheeler et al. [9].

List of symbols

c_u Undrained shear strength

$\boldsymbol{D}$ Elastic stiffness matrix

d Incremental operator

e Void ratio

e_M Void ratio at critical state

f_y Function of the yield surface

H Contractancy function

H_0, H_α, H_χ Hardening moduli

K_{0NC} Coefficient of lateral earth pressure at rest in normally consolidated conditions

K_0 Coefficient of lateral earth pressure

M Slope of the critical state line

n_L Contractancy or additional parameter of the model that controls the shape of the yield surface

p' Mean effective stress

p'_m Preconsolidation pressure

p'_{mi} Intrinsic preconsolidation pressure: $p'_{mi} = p'_m/(1+\chi)$

q Deviatoric stress

α Inclination of the yield surface

$\boldsymbol{\alpha}_\mathbf{d}$ Deviatoric fabric tensor

$\Delta\Lambda$ Plastic multiplier

ε Strain

η Stress ratio: $\eta=q/p'$ or $\boldsymbol{\eta} = \boldsymbol{\sigma}_\mathbf{d} / p'$ (tensor)

κ Slope of swelling line from $v - \ln p'$ space

λ Slope of post yield compression line from $v - \ln p'$ space

λ_i Slope of intrinsic post yield compression line from $v - \ln p'$ space

v Specific volume

ν' Poisson's ratio

ξ, ξ_d Absolute and relative effectiveness of destructuration

σ' Effective stress

ϕ Friction angle

χ Amount of bonding

Ψ Intermediate parameter of the model to simplify equations

ω, ω_d Absolute and relative effectiveness of rotational hardening

CSL Critical state line

NCL Normal compression line

OCR Overconsolidation ratio

Subscripts/superscripts:

0	Initial
d,v	deviatoric, volumetric
e,p	plastic
T	matrix transpose

Table captions

Table 1. Parameters for Kaolin clay [26] and Santa Clara clay [27]

Figure captions

Figure 1. Yield surfaces of the SCLAY1S model [12].

Figure 2. Different shapes of the yield surface for E-SCLAY1S.

Figure 3. E-SCLAY1 yield surface in general stress space (M=1.5, α=0.4).

Figure 4. Euler backward implicit algorithm for the proposed model.

Figure 5. Uniqueness of the CSL.

Figure 6. Undrained triaxial stress paths: (a) With rotational hardening; (b) Without rotational hardening.

Figure 7. Separation between NCL and CSL.

Figure 8. K_{0NC} stress paths.

Figure 9. Isotropic E-SCLAY1: (a) K_{0NC} prediction; (b) Yield surfaces.

Figure 10. Predicion of c_u for isotropically normally consolidated samples.

Figure 11. Deviation in the prediction of yield points in soils with evolving anisotropy.

Figure 12. Yield surfaces for several clays: (a) Winnipeg clay (data after [32]); (b) Otaniemi clay (data after [9]); (c) Drammen clay (data after [33]); (d) Pornic clay (data afer [33]).

Figure 13. Influence of n_L on soil stiffness: (a) Drained triaxial test simulations; (b) Stiffness ratio for confined compression and triaxial stress paths.

Figure 14. Influence of n_L on contractancy under drained shearing at constant mean effective stress (Laboratory data after Hattab and Hicher [34]).

Figure 15. Undrained triaxial stress paths for Kaolin clay (data after [26]).

Figure 16. Isotropically consolidated Kaolin clay (data after [26]): (a) stress–strain and (b) excess pore water pressure.

Figure 17. Isotropically consolidated Santa Clara clay (data after [27]).

Figure 18. K_0-consolidated Santa Clara clay (data after [27]).

Figure 19. Yield surfaces for Bothkennar clay (data after [29]): (a) K_0 and (b) isotropically consolidated.

Figure 20. Reinterpretation of yield zone using arithmetic stress scale. Bothkennar clay, isotropically consolidated samples, compression tests (data after [29]).

Table 1. Parameters for Kaolin clay [26] and Santa Clara clay [27].

Parameters	Kaolin	Santa Clara
M	1.05	1.35
κ	0.05	0.0065
λ	0.14	0.045
ν'	0.2	0.2
e_{ref}*	1.84	1.77
α_{0NC}**	0.40	0.52
ω	≈0	200
ω_d	0.57	0.91

*Reference pressure for the void ratio (1 kPa)
**Using Wheeler et al. [9]

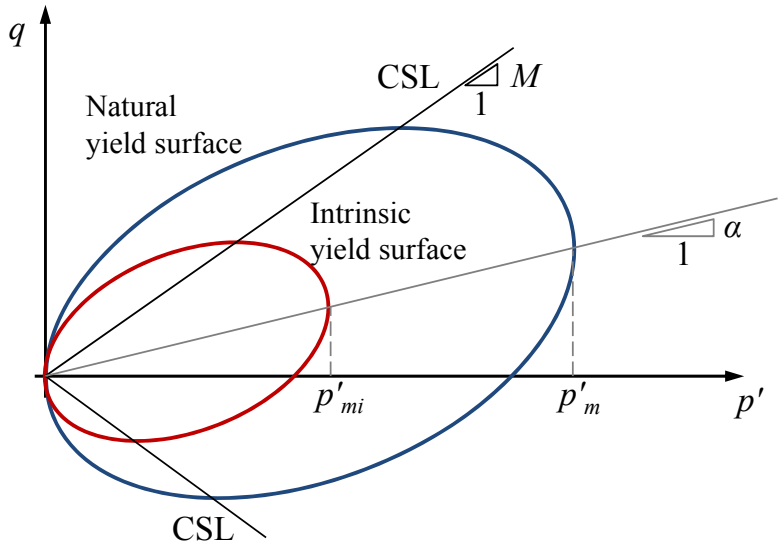

Figure 1. Yield surfaces of the S-CLAY1S model [12].

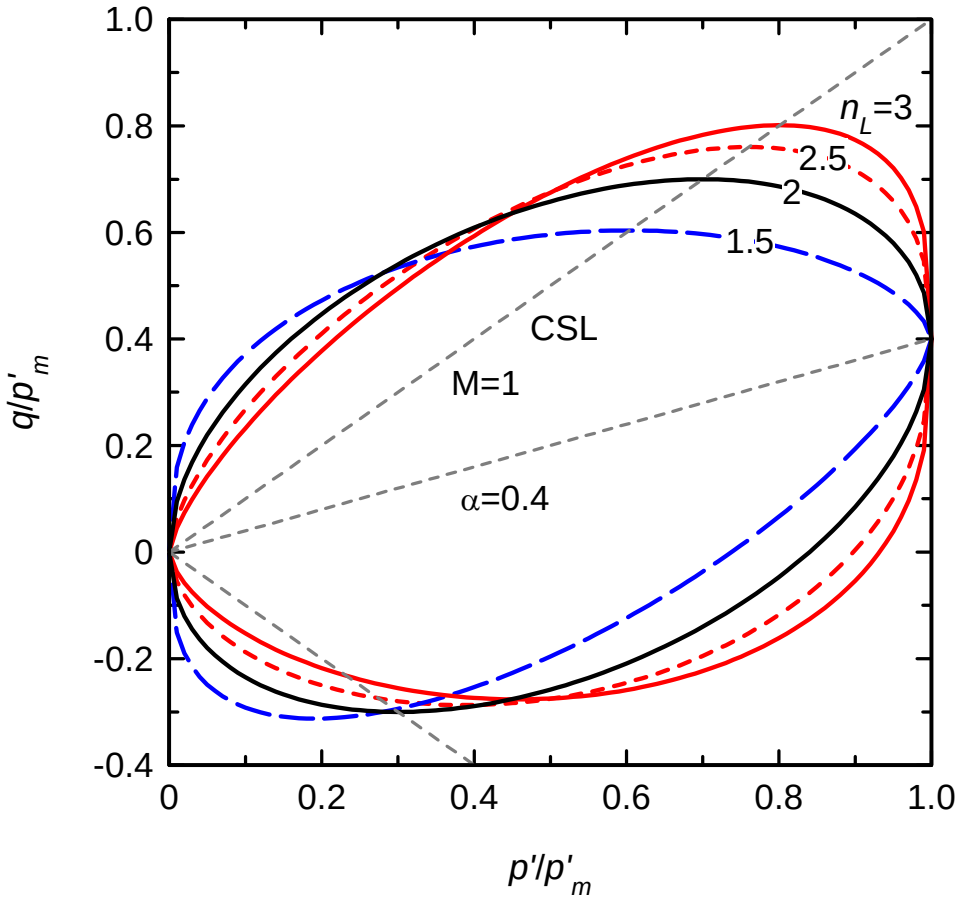

Figure 2. Different shapes of the yield surface for E-SCLAY1.

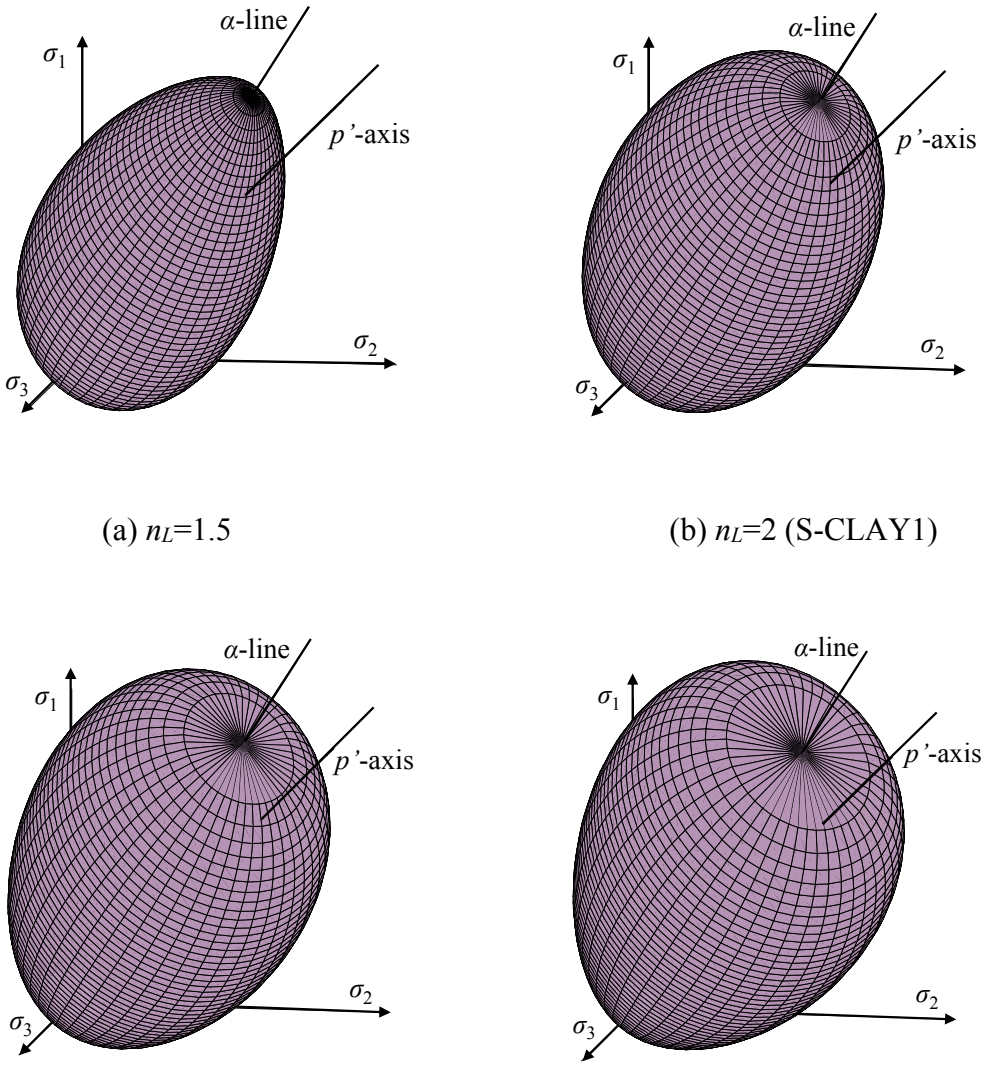

(a) n_L=1.5 (b) n_L=2 (S-CLAY1)

(c) n_L=2.5 (b) n_L=3

Figure 3. E-SCLAY1 yield surface in general stress space (M=1.5, α=0.4).

Get: initial stress $\boldsymbol{\sigma}'_0$, strain increment $d\boldsymbol{\varepsilon}$ and state variables

Calculate $|d\boldsymbol{\varepsilon}|$

If ($|d\boldsymbol{\varepsilon}| < 0.1\%$) determine sub increment 'n_sub'

Subdivide strain increment $d\boldsymbol{\varepsilon}^n = d\boldsymbol{\varepsilon} / n\_sub$

End If

Do i = 1, n_sub

$d\boldsymbol{\varepsilon}^t = d\boldsymbol{\varepsilon}^n$ and $d\boldsymbol{\varepsilon}^p = 0$

converged = .false.

While *(not converged)* Do

$d\boldsymbol{\varepsilon}_i^t = d\boldsymbol{\varepsilon}_{i-1}^t - d\boldsymbol{\varepsilon}_{i-1}^p$

$d\boldsymbol{\sigma}_i^t = \boldsymbol{D} d\boldsymbol{\varepsilon}_i^t$

$\boldsymbol{\sigma}_i^t = \boldsymbol{\sigma}_0^t + d\boldsymbol{\sigma}_i^t$

Calculate f_y (yield function)

If ($f_y < 1\times10^{-7}$) Then

Purely elastic behaviour, Return

converged = .true.

End If

If ($f_y \geq 1\times10^{-7}$) Then

Calculate plastic multiplier $d\Lambda$ in Eq. (13)

Calculate plastic strains $d\boldsymbol{\varepsilon}^p$

Update state variables

converged = .false.

End If

End While

End Do

Return

Figure 4. Euler backward implicit algorithm for the proposed model

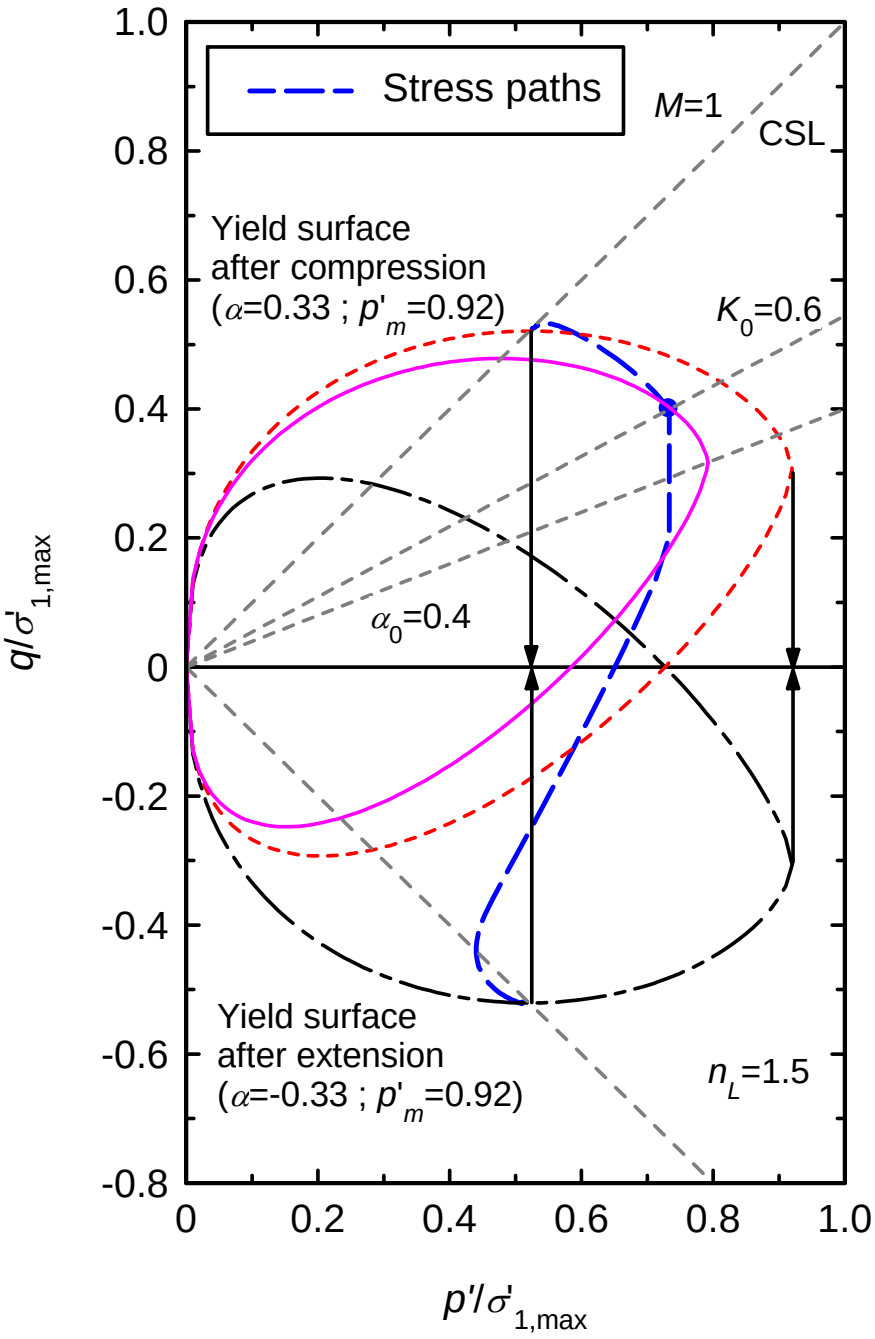

Figure 5. Uniqueness of the CSL.

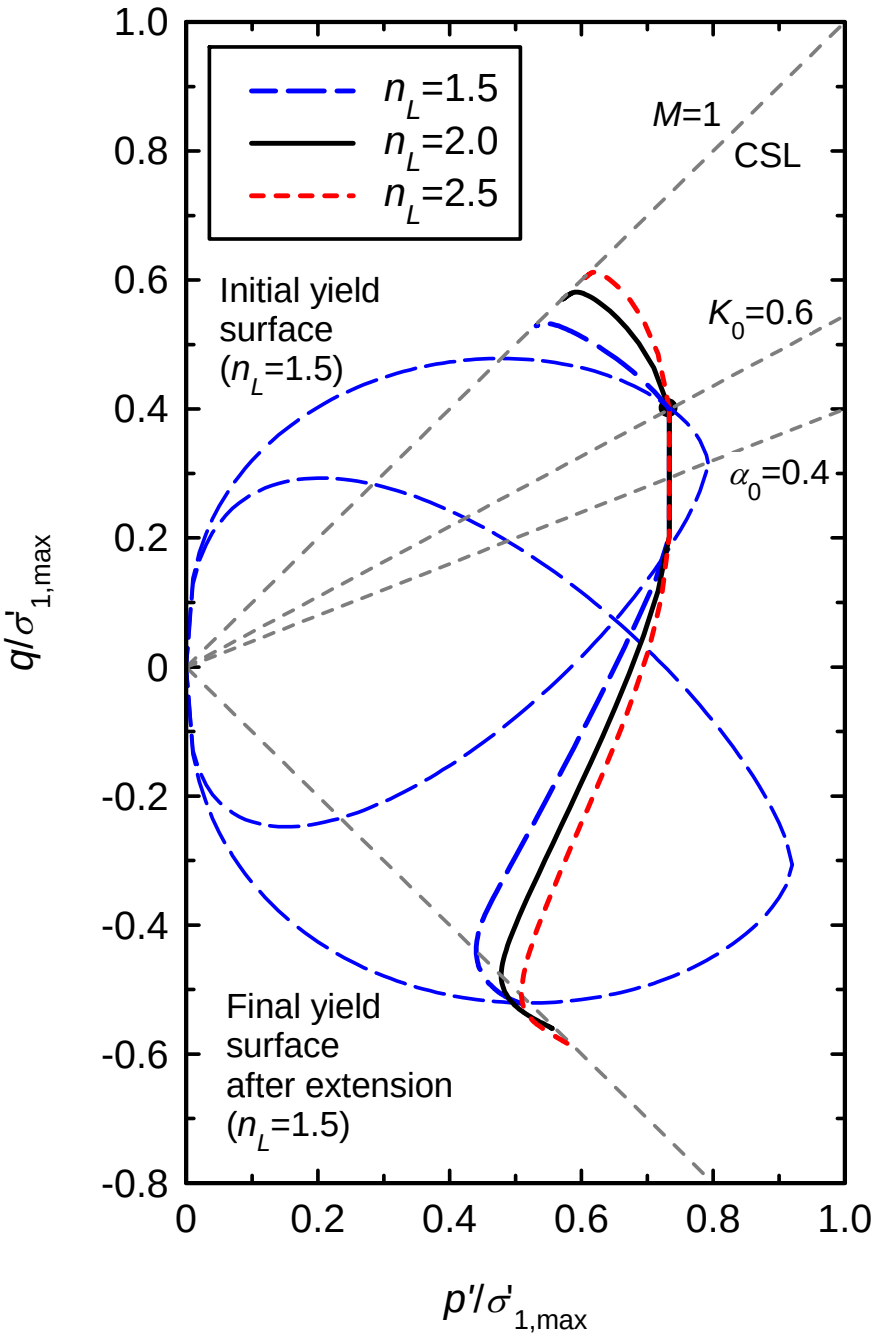

(a) With rotational hardening

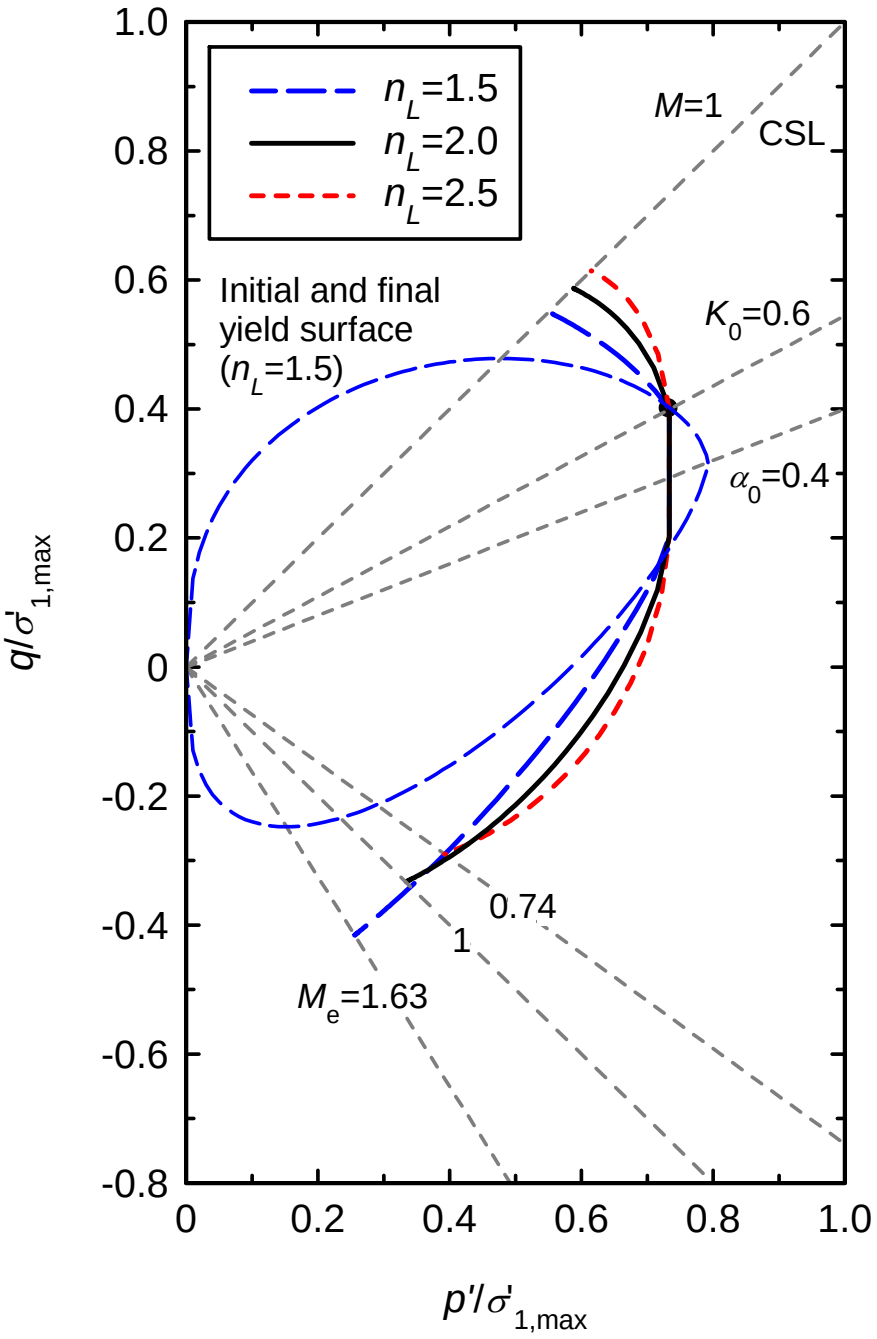

(b) Without rotational hardening

Figure 6. Undrained triaxial stress paths.

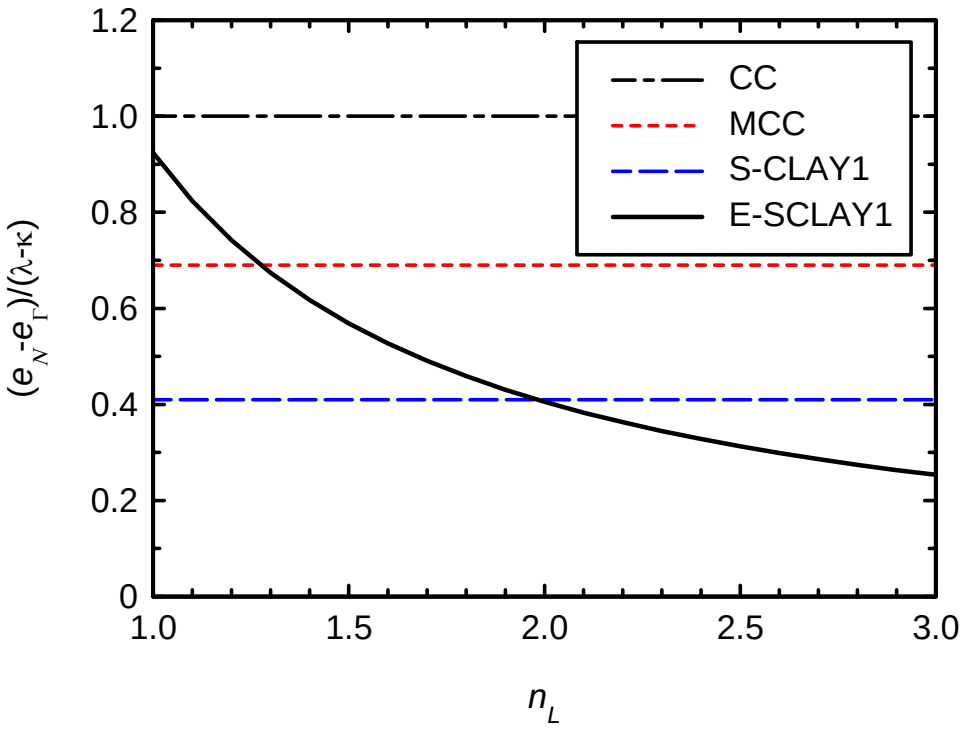

Figure 7. Separation between NCL and CSL.

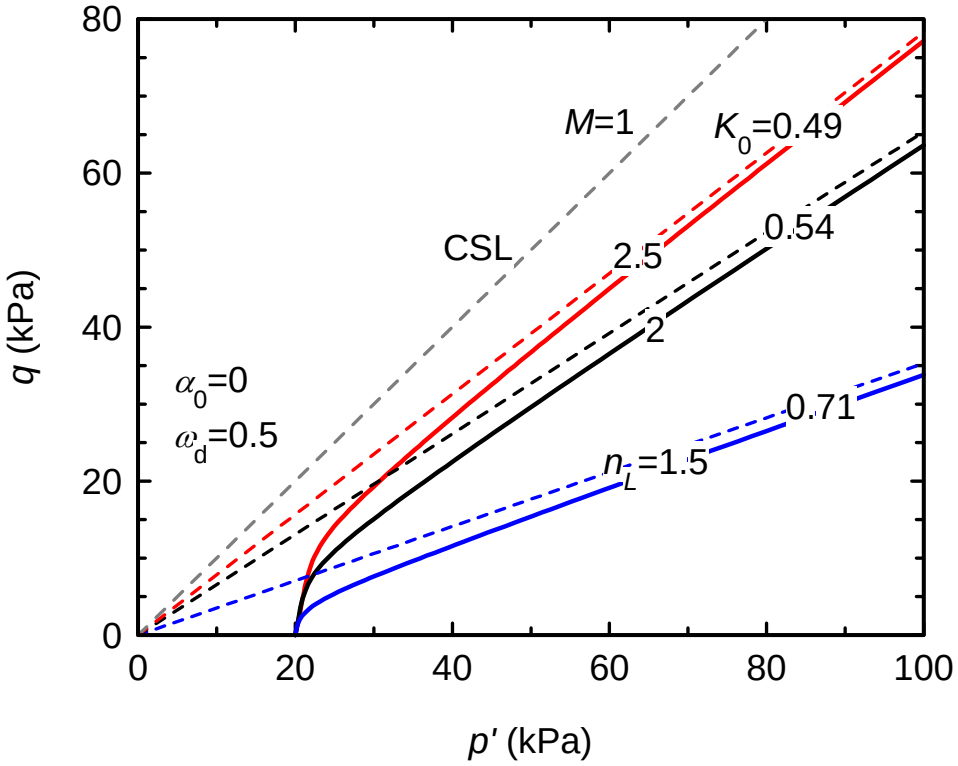

Figure 8. K_{0NC} stress paths.

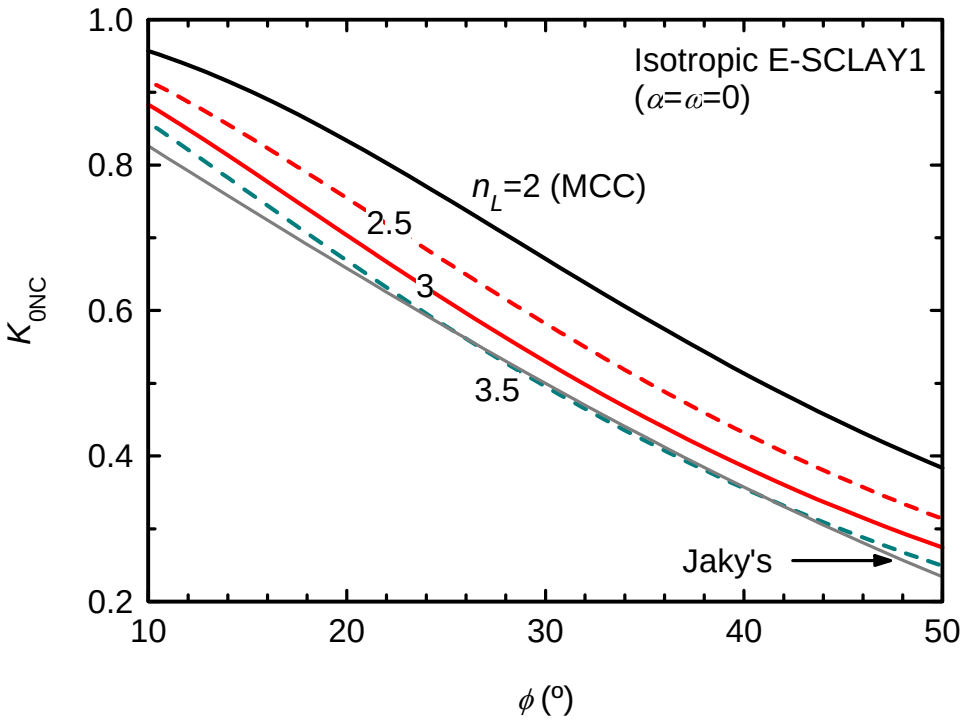

(a)

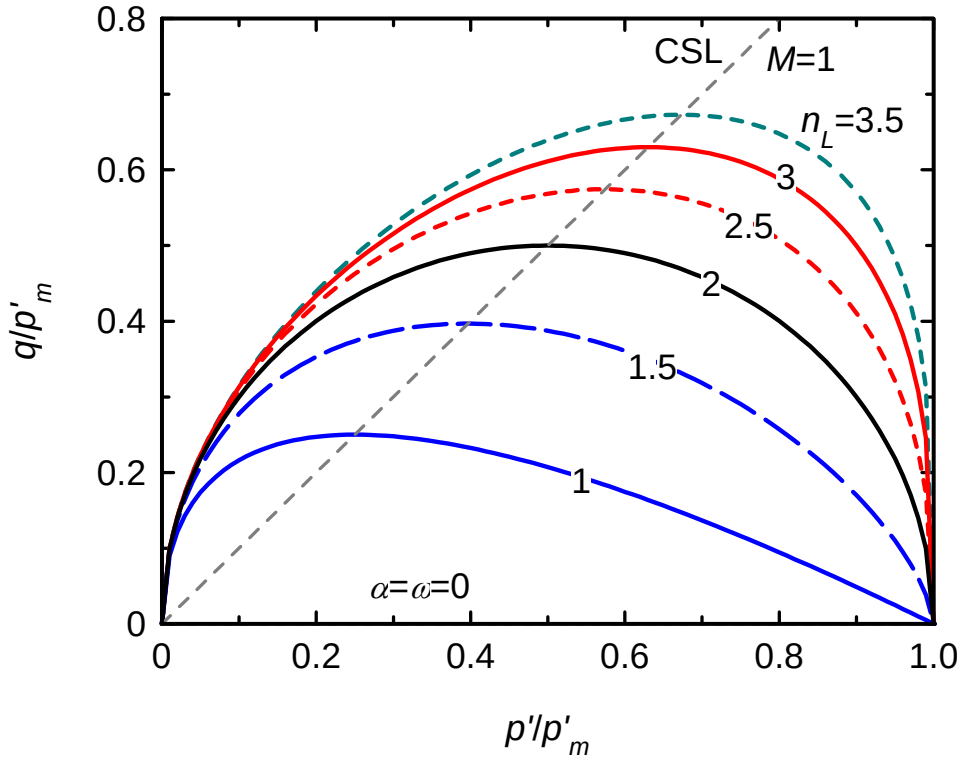

(b)

Figure 9. Isotropic E-SCLAY1: (a) K_{0NC} prediction; (b) Yield surfaces.

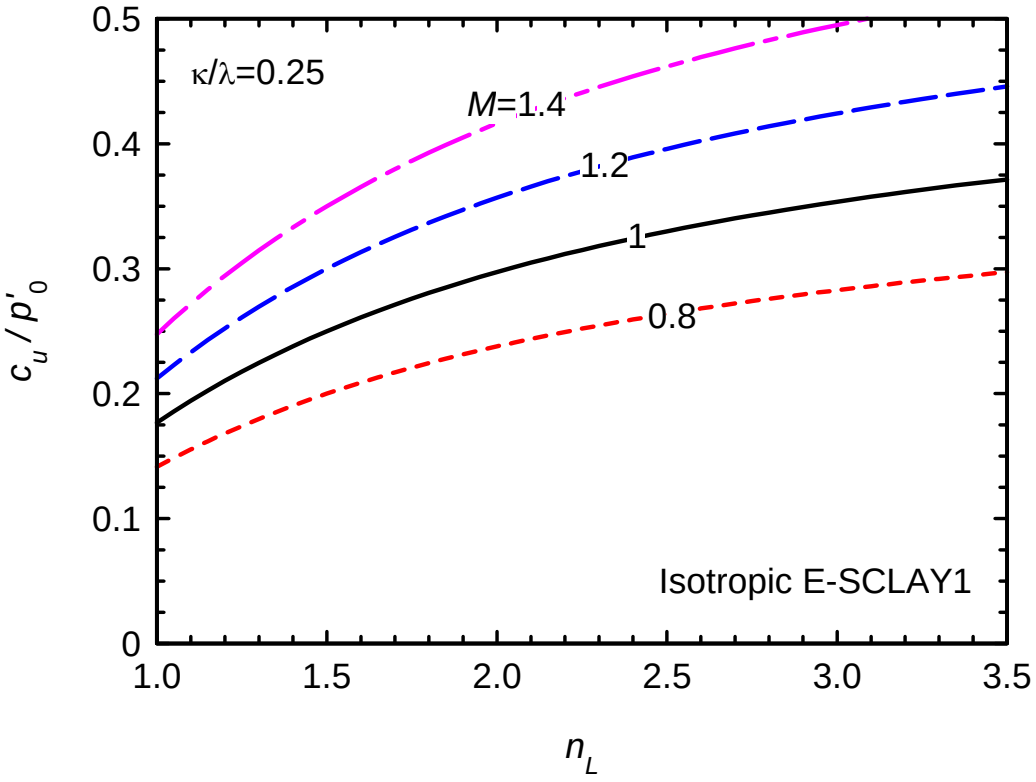

Figure 10. Predicion of c_u for isotropically normally consolidated samples.

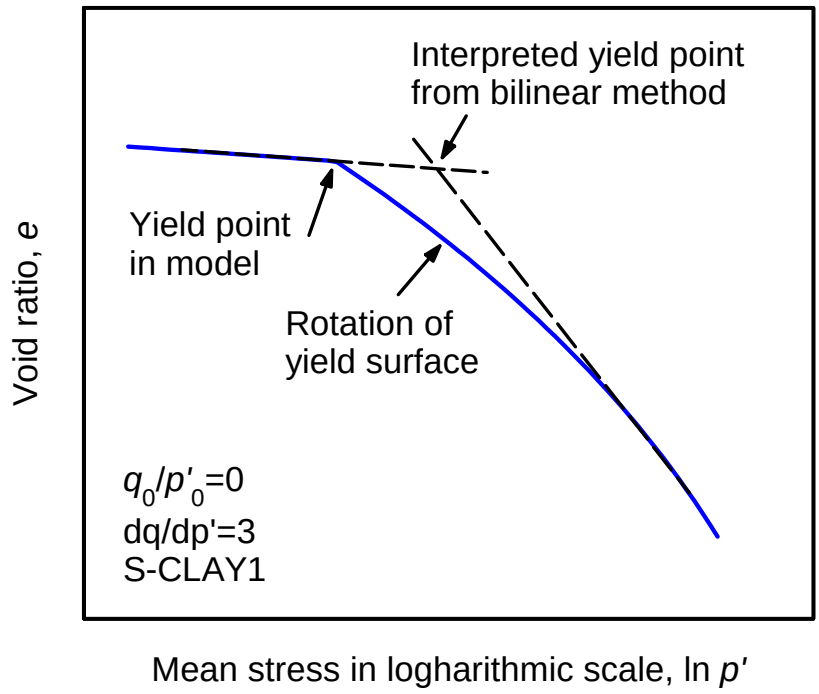

Figure 11. Deviation in the prediction of yield points in soils with evolving anisotropy.

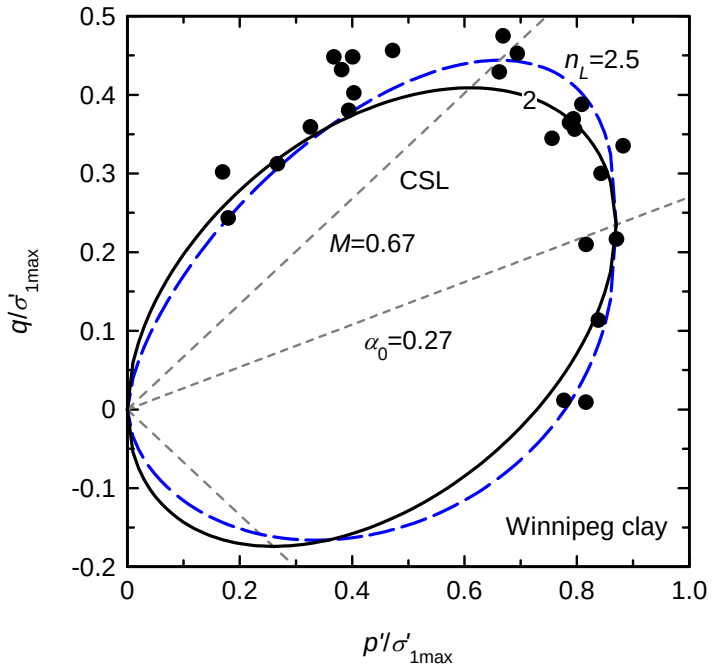
0.5
0.4
0.3
0.2
0.1
0
-0.1
-0.2
0
0.2
0.4
0.6
0.8
1.0
q/σ'_{1max}
p'/σ'_{1max}
n_L=2.5
2
CSL
M=0.67
α_0=0.27
Winnipeg clay

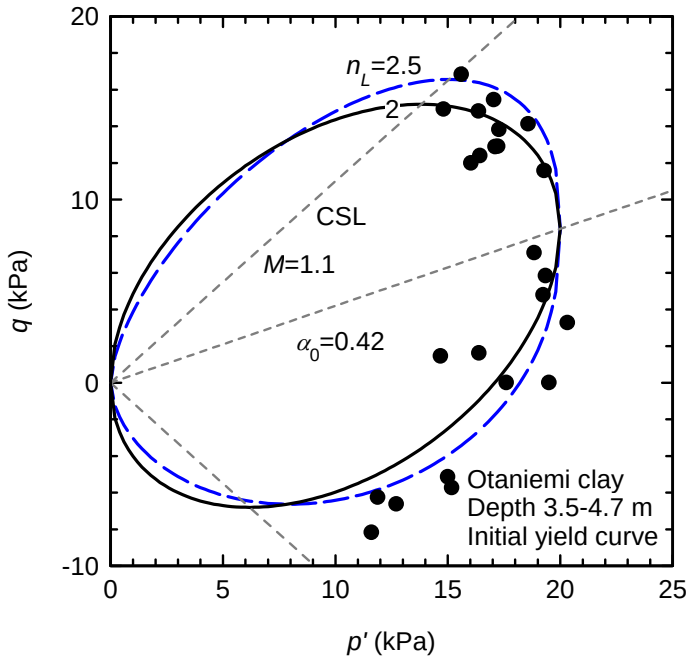
20
10
0
-10
0
5
10
15
20
25
q (kPa)
p' (kPa)
n_L=2.5
2
CSL
M=1.1
α_0=0.42
Otaniemi clay
Depth 3.5-4.7 m
Initial yield curve

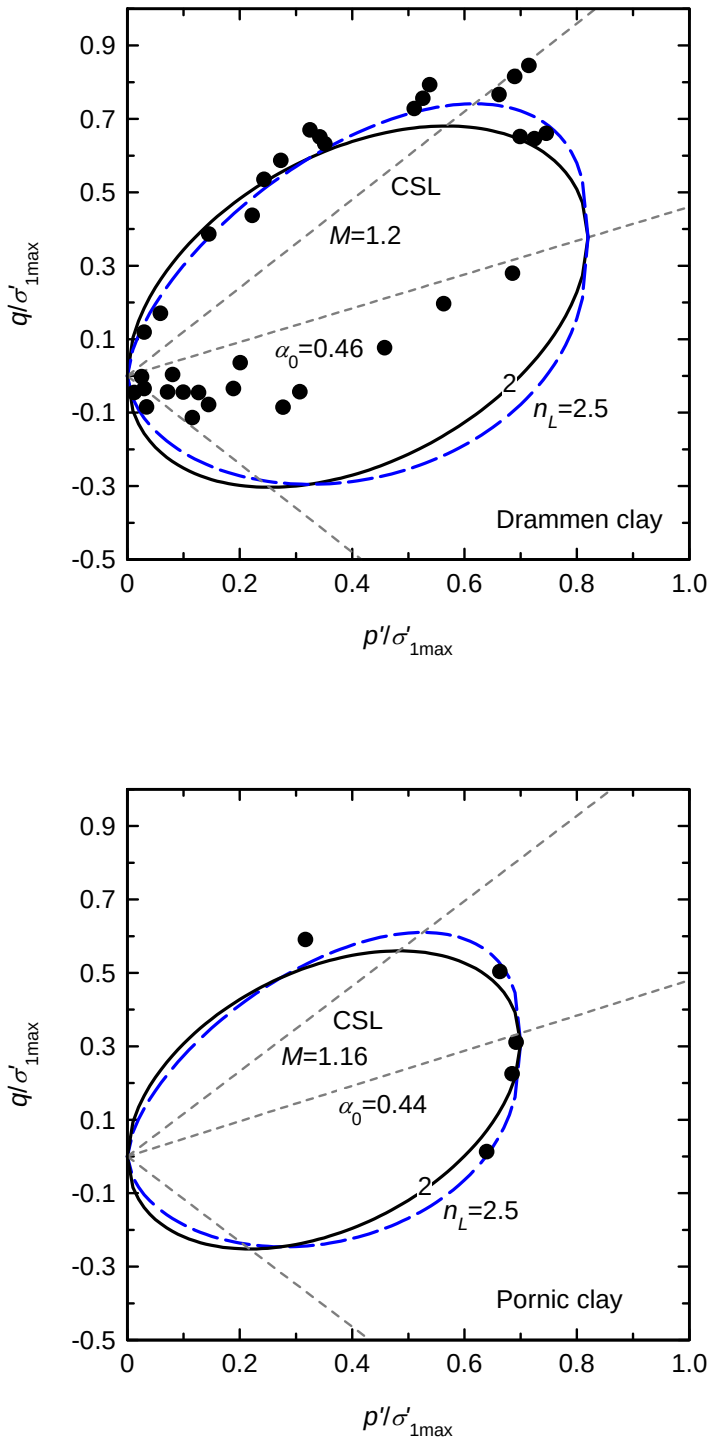

Figure 12. Yield surfaces for several clays: (a) Winnipeg clay (data after [32]); (b) Otaniemi clay (data after [9]); (c) Drammen clay (data after [33]); (d) Pornic clay (data afer [33]).

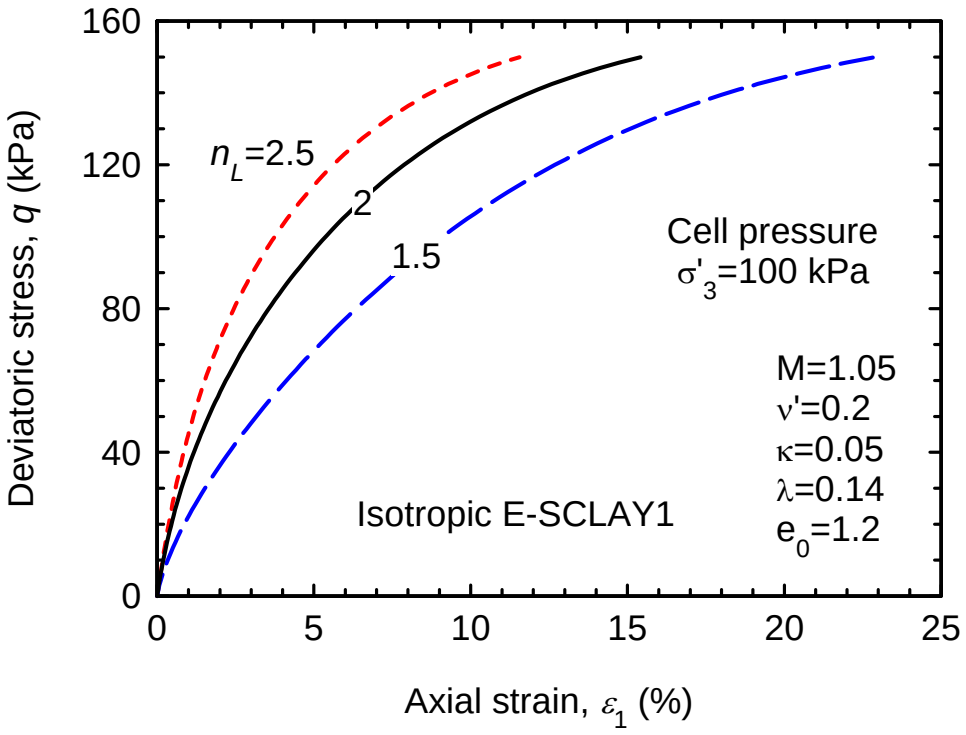

(a)

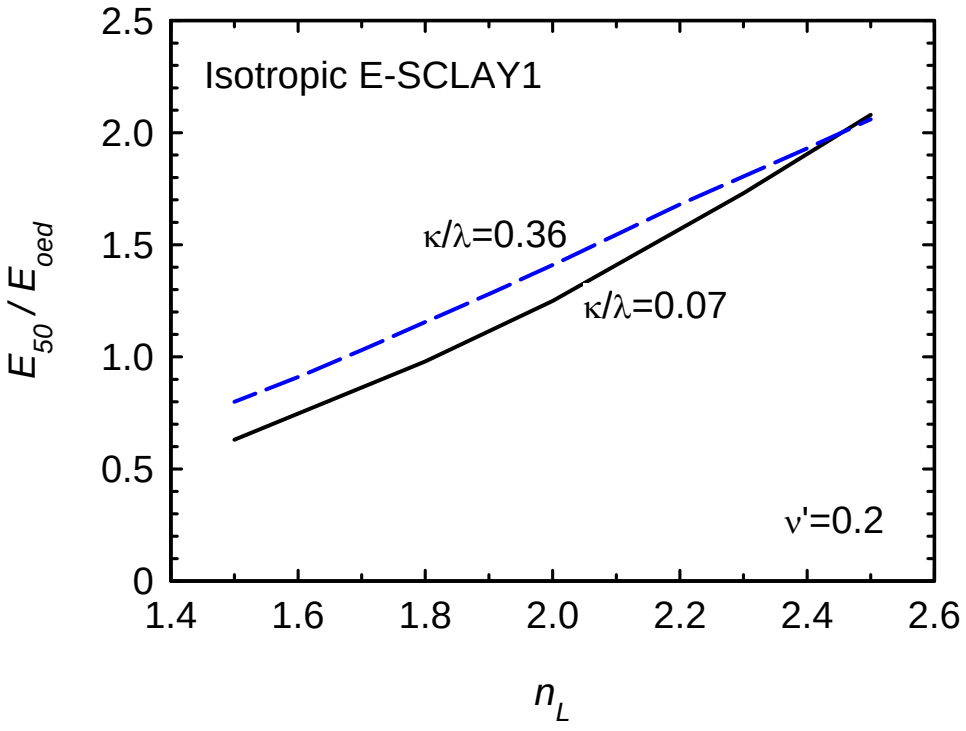

(b)

Figure 13. Influence of n_L on soil stiffness: (a) Drained triaxial test simulations; (b) Stiffness ratio for confined compression and triaxial stress paths.

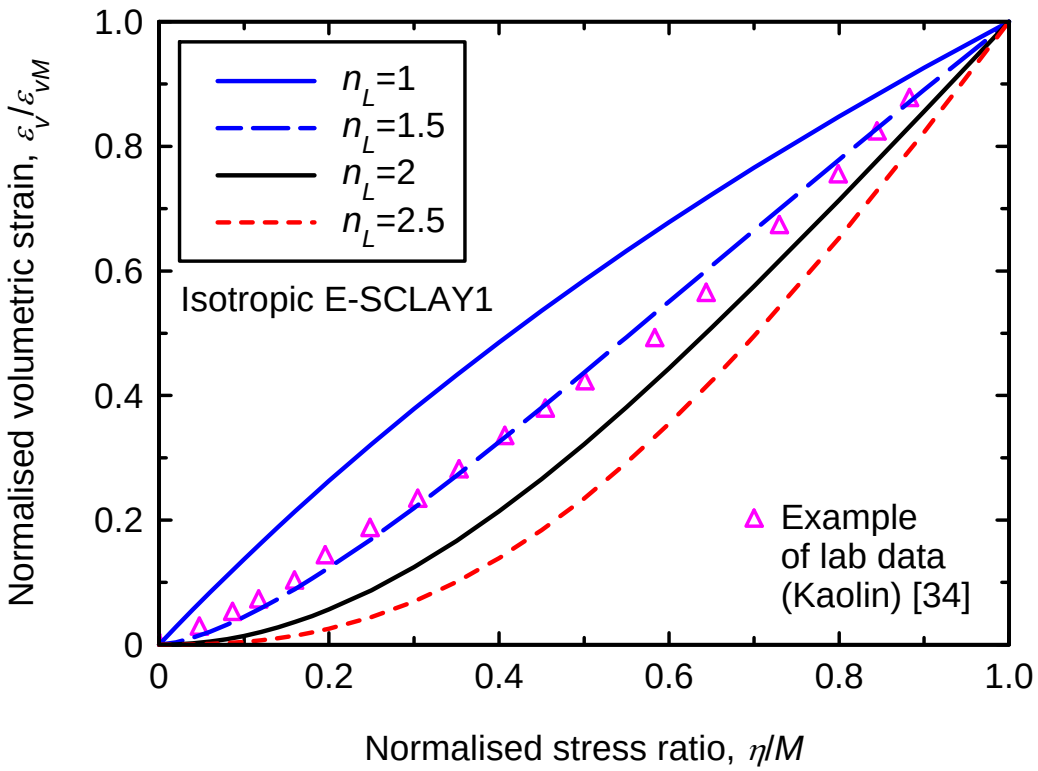

Figure 14. Influence of n_L on contractancy under drained shearing at constant mean effective stress (Laboratory data after Hattab and Hicher [34]).

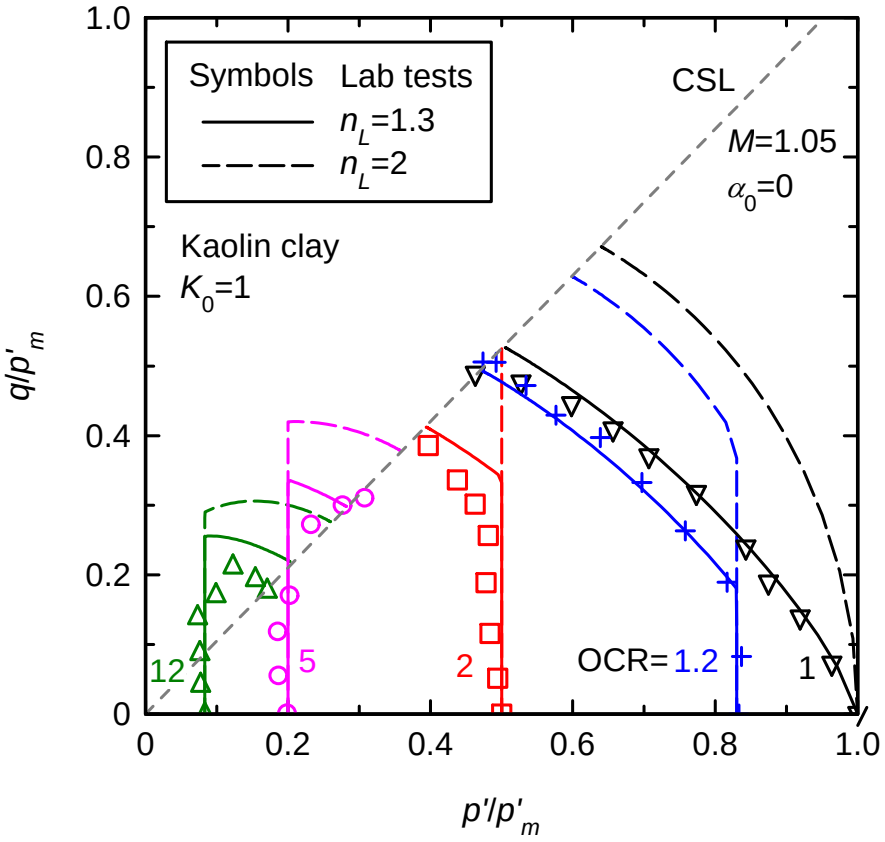
Symbols Lab tests
n_L=1.3
n_L=2
Kaolin clay
K_0=1
CSL
M=1.05
α_0=0
OCR= 1.2
12
5
2
1
q/p'_m
p'/p'_m

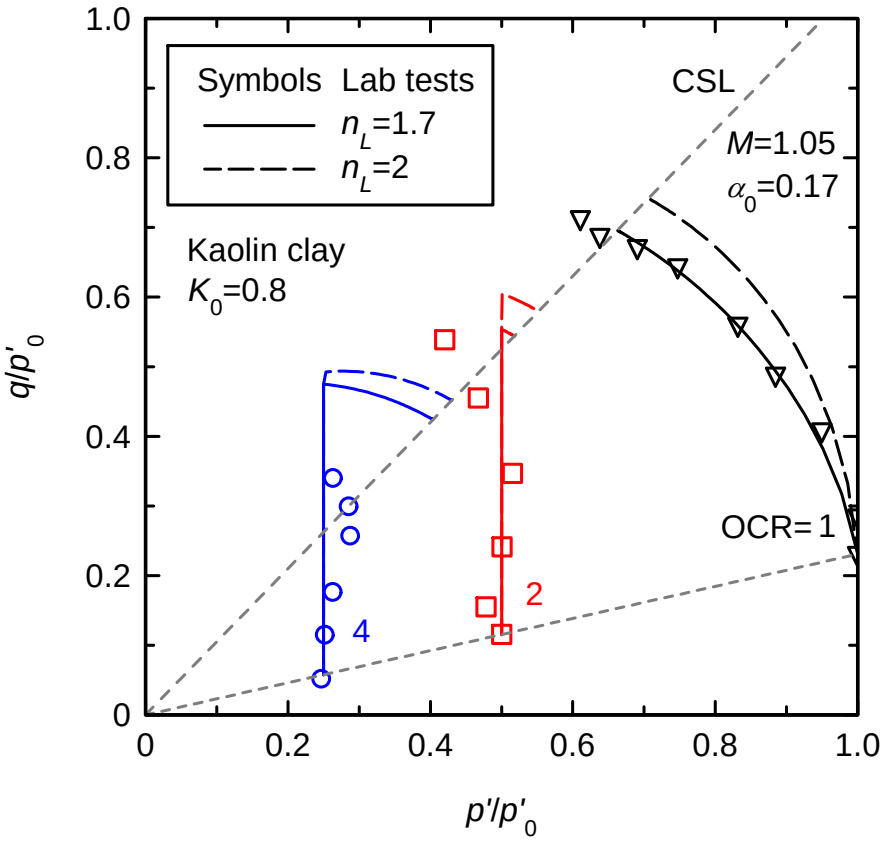
Symbols Lab tests
n_L=1.7
n_L=2
Kaolin clay
K_0=0.8
CSL
M=1.05
α_0=0.17
OCR= 1
4
2
q/p'_0
p'/p'_0

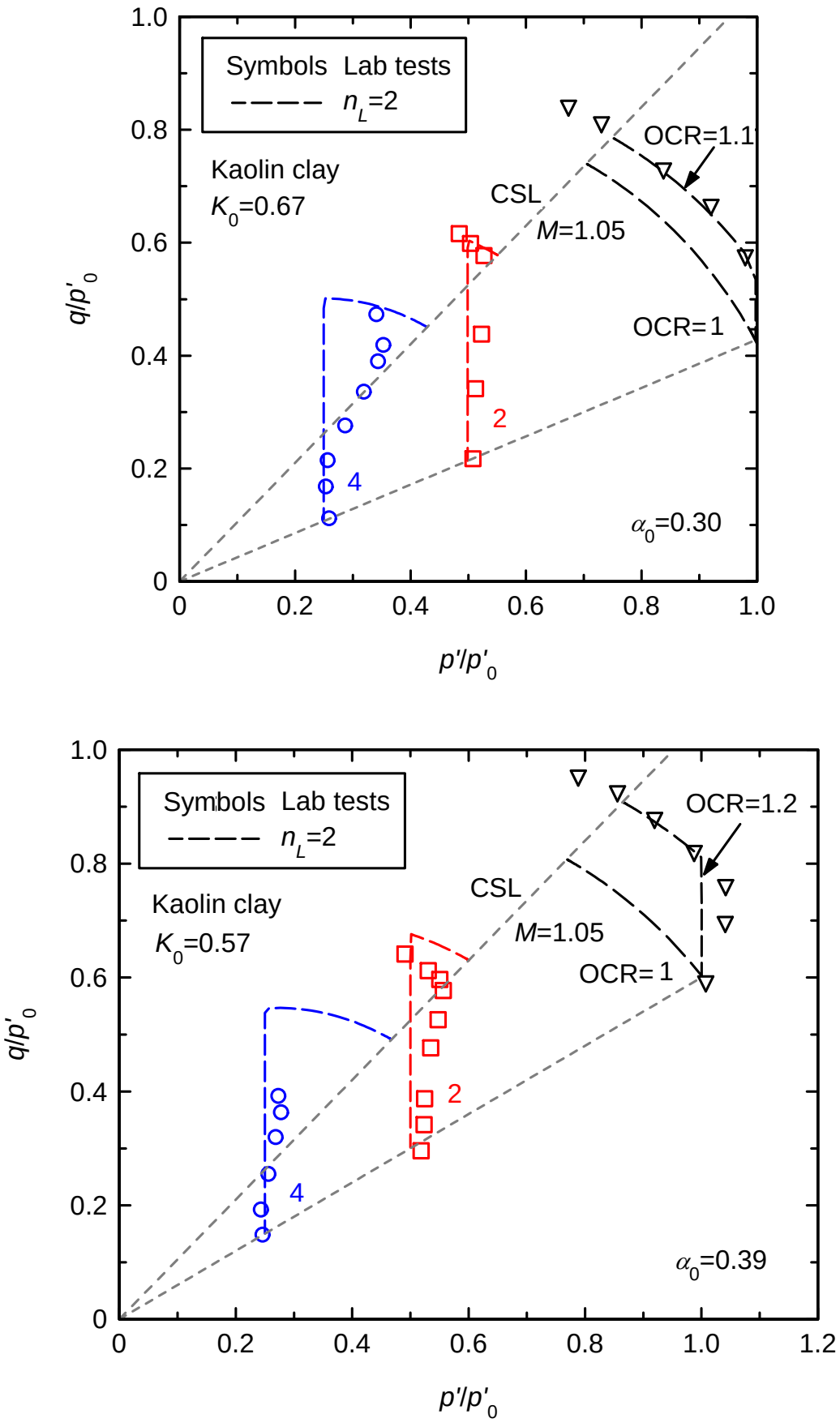

Figure 15. Undrained triaxial stress paths for Kaolin clay (data after [26]).

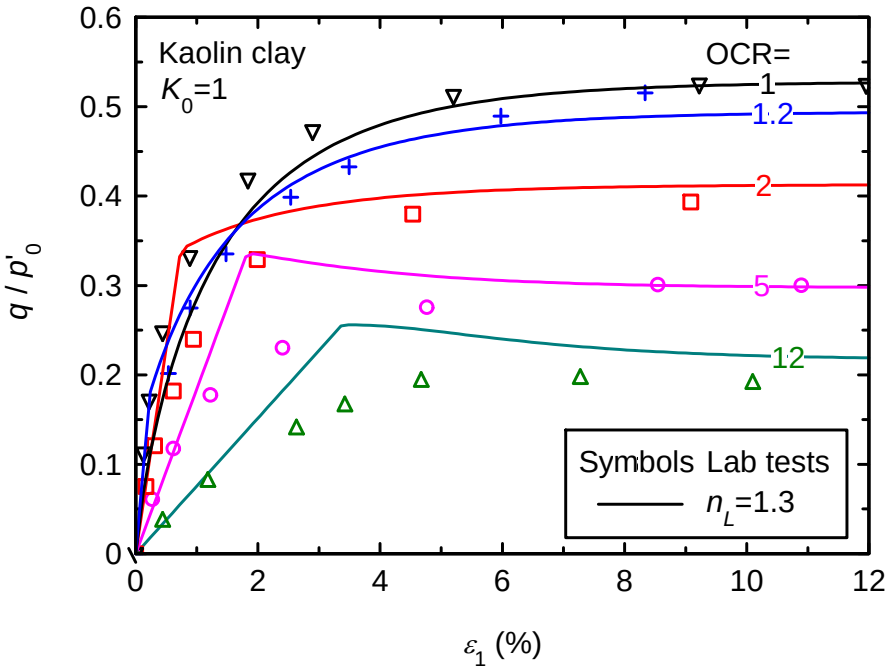

(a)

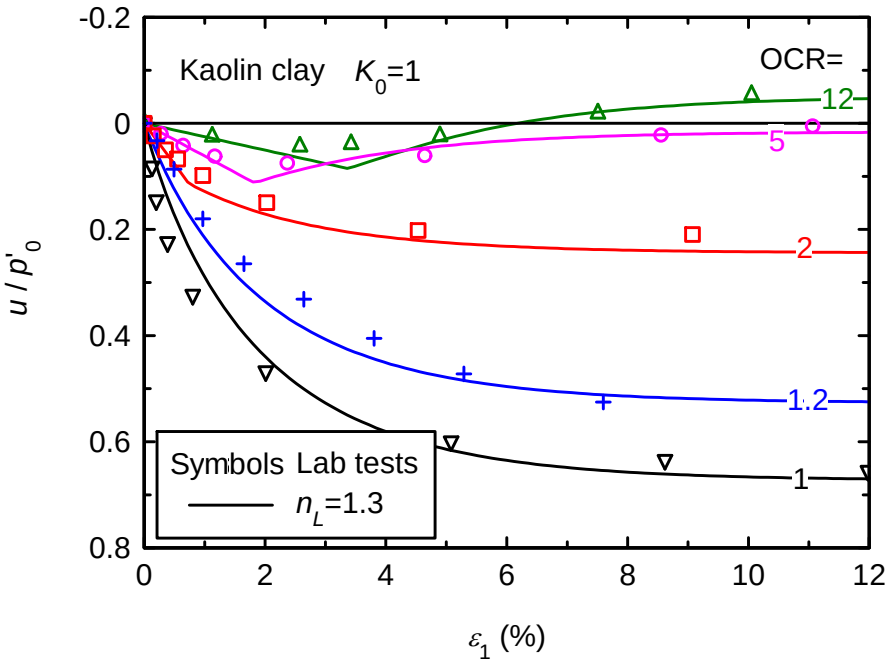

(b)

Figure 16. Isotropically consolidated Kaolin clay (data after [26]): (a) stress–strain and (b) excess pore water pressure.

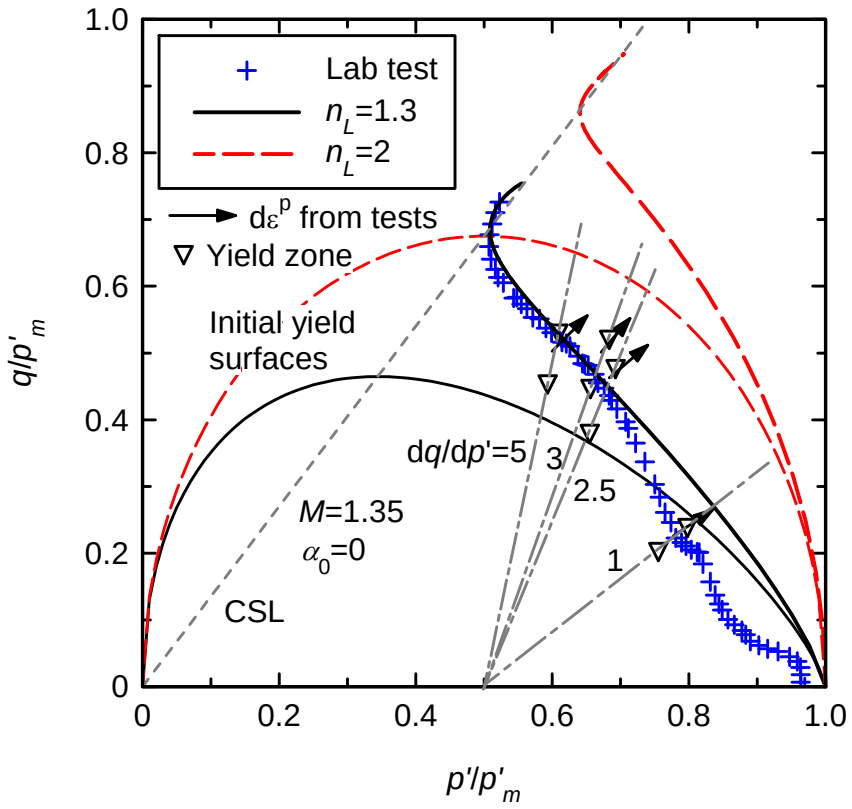

Figure 17. Isotropically consolidated Santa Clara clay (data after [27]).

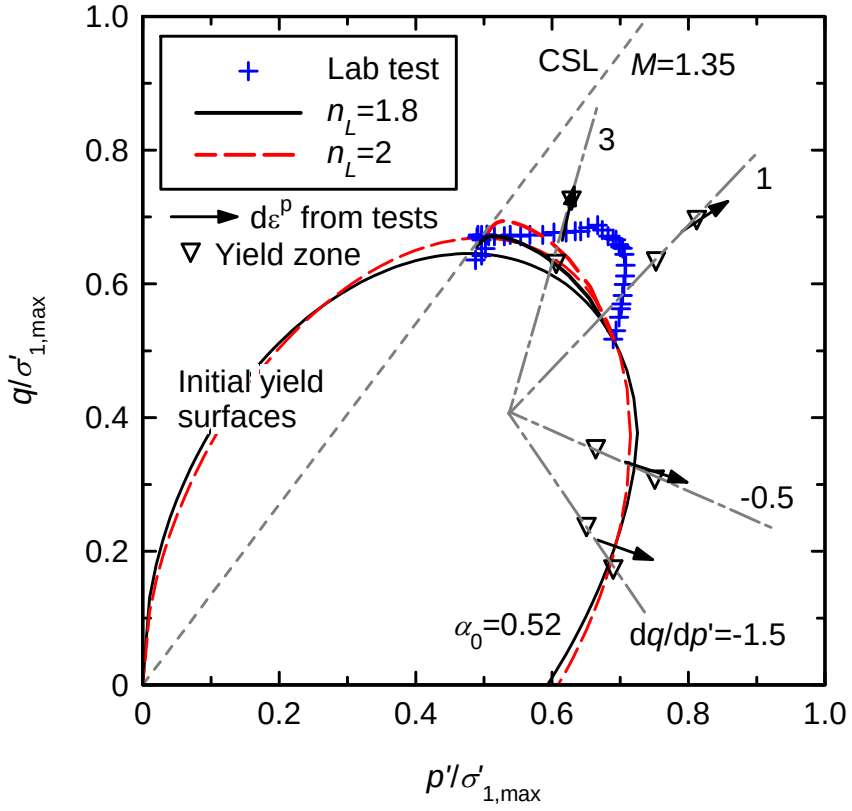

Figure 18. K_0-consolidated Santa Clara clay (data after [27]).

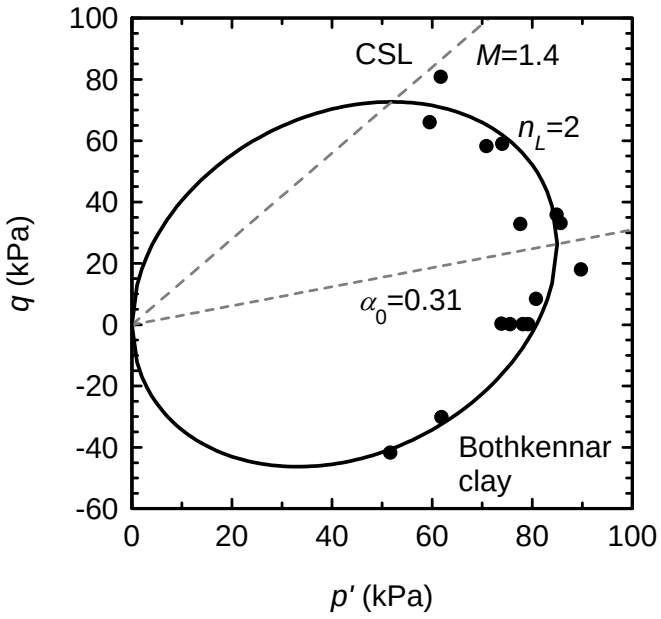

(a)

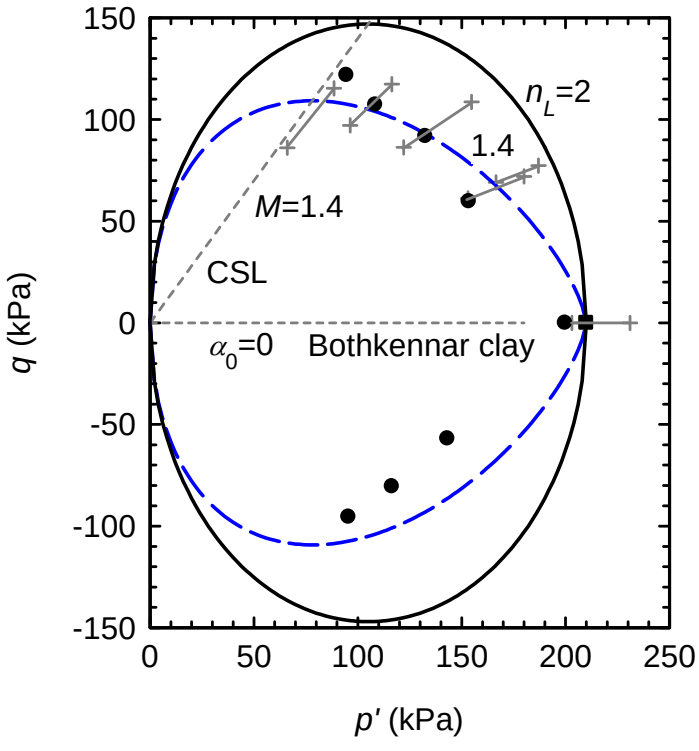

(b)

Figure 19. Yield surfaces for Bothkennar clay (data after [29]): (a) K_0 and (b) isotropically consolidated.

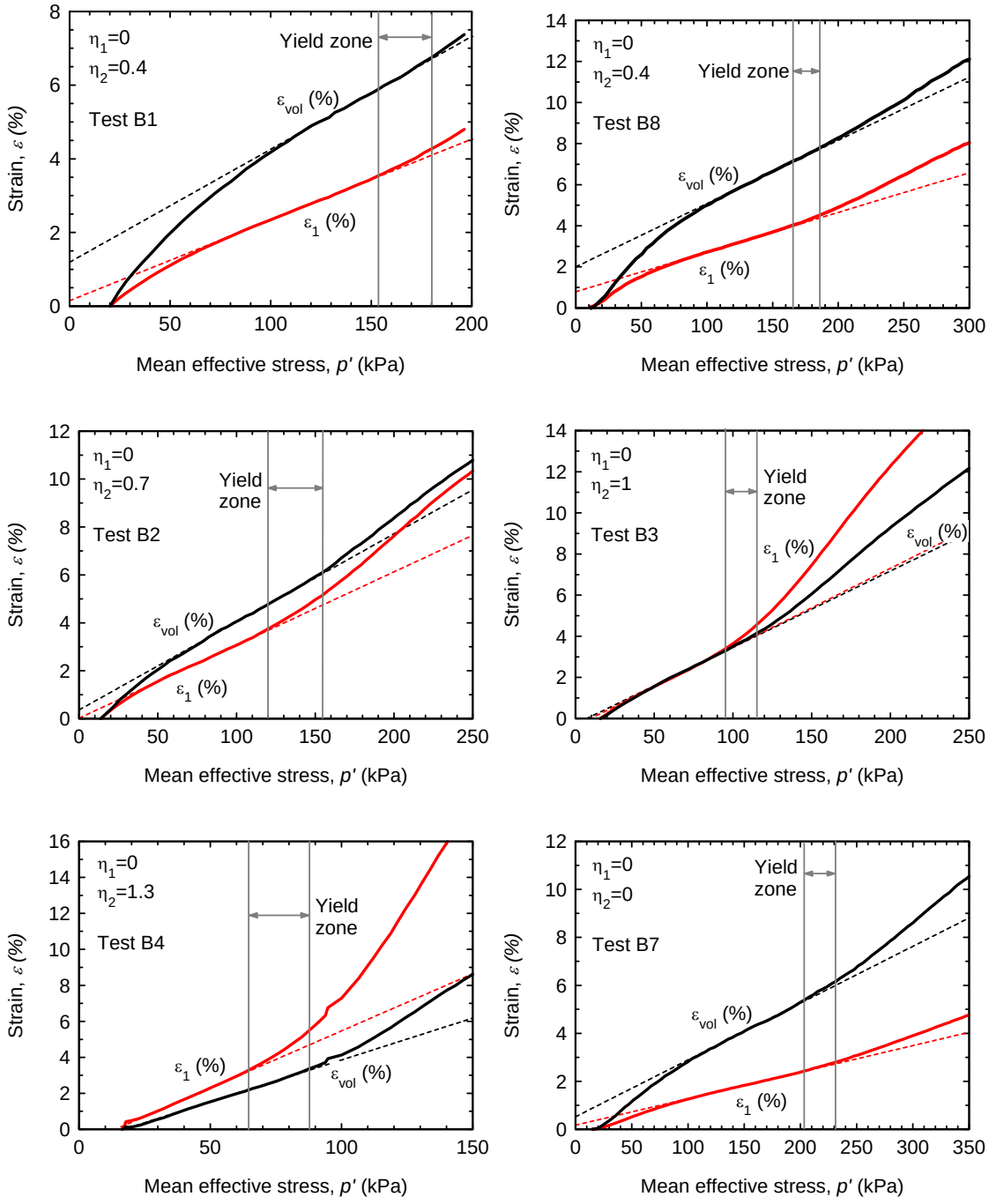

Figure 20. Reinterpretation of yield zone using arithmetic stress scale. Bothkennar clay, isotropically consolidated samples, compression tests (data after [29]).